Aalto-yliopisto
Aalto-universitetet
Aalto University

Master´s Programme in Geoinformatics

Geodetic Synthetic Aperture Radar in Finland

Mahnoor Fatima

Master’s thesis
2023

Aalto-yliopisto
Aalto-universitetet
Aalto University

Master’s thesis
2023

Aalto-yliopisto
Aalto-universitetet
Aalto University

Author Mahnoor Fatima

Title of thesis Geodetic Synthetic Aperture Radar in Finland

Programme Master's programme in Geoinformatics

Major Geoinformatics

Thesis supervisor Professor Maaria Nordman

Thesis advisor(s) Professor Maaria Nordman

Date 30.10.2023 **Number of pages** 62 **Language** English

Abstract

Synthetic Aperture Radar (SAR) is a powerful remote sensing technology that provides detailed images of larger areas, regardless of weather conditions or daylight. This study delves into the efficacy and performance of passive corner reflectors deployed in Finland, with a specific focus on their suitability for Synthetic Aperture Radar (SAR) calibration. The corner reflectors, strategically positioned across diverse sites, offer a cost-effective and low-maintenance alternative to active transponders. However, their large size and weight, particularly in longer wavelengths, present challenges in deployment, and their autonomous settling effect may introduce distortions in deformation measurements. This research rigorously examined the precision and reliability of these reflectors, addressing their response to varying weather conditions and potential geometric alterations over extended deployment periods. Two reflectors, situated in Metsähovi and Loviisa, both characterized by a triangular trihedral design were chosen for comparative analysis. The study was conducted from September 2022 to June 2023 and is investigated the influence of snow depth and temperature on signal to clutter ratio values. It also examined how corner reflectors behave under various weather conditions. This research can provide insights into the utilization of corner reflectors for SAR calibration, guiding future applications in geodetic measurements and large-scale processes.

Keywords SAR, Corner reflectors, SCR values, snow depth, CR´s positioning

Master's thesis
2023

Aalto-yliopisto
Aalto-universitetet
Aalto University

Table of Contents

Aalto-yliopisto
Aalto-universitetet
Aalto University

Aalto-yliopisto
Aalto-universitetet
Aalto University

List of Figures

List of tables

List of Abbreviations

SAR	Synthetic Aperture Radar
HH	Horizontal- Horizontal polarization
VV	Vertical-Vertical polarization
HV	Horizontal-Vertical polarization
VH	Vertical-Horizontal polarization
SCR	Signal to clutter ratio
CR	Corner reflector
ITRF	International Terrestrial Reference Frame
SLC	Single Look Complex

Aalto-yliopisto
Aalto-universitetet
Aalto University

Preface and acknowledgements

I want to thank Professor Maaria Nordman, Professor Jaan Praks, Marius Schlaak Jyri Näränen and Arttu Raja-Halli for their good advice and guidance.

I also want to thank my mother for her immense support.

Otaniemi, 2023
Mahnoor Fatima Student

Aalto-yliopisto
Aalto-universitetet
Aalto University

1.Introduction

Remote sensing is a scientific and technological field which is primarily focused on acquiring measurements of extensive objects through aerial and space-based platforms. It serves as a crucial method for obtaining insights into large scale planetary processes. Its diverse applications include assessment of extensive land areas, aquatic environments, atmospheric conditions, and large-scale human activities.

Many remote sensing instruments function in the visible and microwave ranges of the electromagnetic spectrum because those wavelengths have the advantage of effectively passing through the Earth's atmosphere. This is related to microwave radar technology, particularly Synthetic Aperture radar (SAR), which is being researched actively these days. SAR instruments offer a range of imaging modes, including multi polarization, where signals are transmitted and received in various polarizations. Additionally, there is the multi frequency mode that employs radar signals at different wavelengths to gather data, along with the multi antenna imaging mode, whereas SAR systems utilize multiple antennas or apertures to simultaneously capture data from slightly different angles (Praks, 2012).

To conduct precise quantitative temporal and spatial analysis of SAR data, it is essential to perform calibration. This process guarantees that the recorded pixel values of both amplitude and phase align accurately with the actual geophysical parameters being studied. Corner reflectors, due to their distinctive characteristics, serve as reliable targets for SAR calibration. They offer notable advantages, exhibiting a considerable return signal magnitude relative to their size. Furthermore, they demonstrate insensitivity to alignment errors, making them a reliable choice. Corner reflectors also present cost effectiveness in terms of both production and maintenance (Garthwaite et al., 2015).

Additionally, corner reflectors have also been used in many geodetic measurements. They have played a pivotal role in initiatives such as height system unification (Gruber et al., 2022), facilitating the integration of measurements obtained through interferometric Synthetic Aperture Radar and Global Navigation Satellite System techniques (Garthwaite et al., 2015). Moreover, they have been used in monitoring nonlinear and fast deformations induced by e.g., subterranean mining activities (Filipiak et al., 2023) and accurately gauging crustal deformation from space (Garthwaite et al., 2013).

1.1. Research Problem

However, Corner reflectors also have a few drawbacks. These reflectors present challenges due to their size and weight, particularly in longer wavelengths such as C band which is used by SAR. Due to having large size and heavy weight it is difficult to transport them especially in areas with restricted accessibility. Moreover, their settling effect due to their weight can introduce distortions in the recorded deformation signal. Prolonged deployment further exposes these structures to potential disturbances and geometric alterations brought about by fluctuating weather and thermal conditions. Thus, before employing corner reflectors for SAR calibration, a rigorous validation of their precision and reliability is needed.

1.2. Motivation

1.2.1 Efficiency assessment of Deployed Corner Reflectors in Finland

As part of testing new geodetics infrastructure, various agencies in Nordic countries, including Finland's FGI (Finnish Geospatial Research Institute) have started installing passive reflectors. Presently, nine reflectors have been deployed across different sites in Finland (see figure 1.1). These are passive corner reflectors having trihedral triangular design, which is a proven design with a larger opening angle and were built robustly so that they can work well during snow. Significantly, they present benefits of being low maintenance and cost effective in contrast to active devices such as transponders. The selection of sites for these corner reflectors is chosen carefully, allowing multiple stations to be within the same SAR swath, as exemplified by Sentinel 1 swaths in Figure 1.

Once corner reflectors were installed by FGI, the next target was to assess their efficiency and address potential drawbacks. For this purpose, it was necessary to observe their signal to clutter ratio (SCR)values, which is the measure of radar signal's strength reflected from target in relation to surrounding clutter.

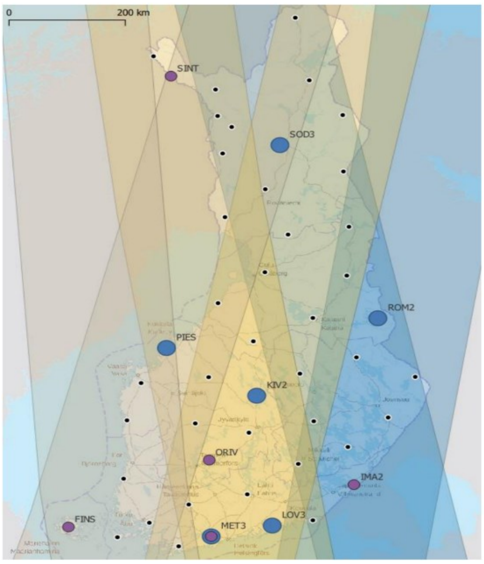

Figure 1: Finland sites where corner reflectors are installed shown in blue dots. Red dots indicate corner reflectors that installed recently. The yellow and blue swaths are the ones covered by Sentinel-1 in ascending and descending tracks.

In this research, two corner reflectors in Finland were studied, one located in Metsähovi, installed in 2010 and the other in Loviisa, installed in December 2021. Both have the same triangular trihedral design with a 1.5-meter inner leg length. The objective was to compare SCR values between these two reflectors and examine the influence of snow depth and temperature on their efficiency. The study period spans from September 2022 to June 2023.

1.3. Research Questions

The research questions are:

1. What is the impact of snow depth on SCR values of corner reflectors at the selected sites (Loviisa and Metsähovi) in varying weather conditions?
2. How do the corner reflectors at Loviisa and Metsähovi sites can be compared in terms of their efficiency and performance in SAR imagery?

2. Synthetic Aperture Radar (SAR)

This chapter gives an overview of SAR explaining its background, basic principles along with applications in Earth observation and comparison of SAR with optical data in different fields.

2.1. Background of SAR Technology

In recent decades, progress in remote sensing technology has resulted in the launch of a range of satellites including multispectral, hyperspectral, and synthetic aperture satellites. Unlike traditional optical sensors, SAR is highly resilient to external disturbances and possesses excellent penetration capabilities. The recent high resolution SAR satellites, such as RADARSAT-2, COSMO-Skymed, TerraSAR-X/TanDEM-X, and more recently Sentinel-1, have notably improved the accuracy of geometric detail in weather independent and daytime remote sensing. In numerous scientific disciplines, SAR observations have become invaluable for studying and monitoring changes on earth's surface (Marinkovic et al., 2007).

SAR is a radar system that operates in a side-looking manner, effectively simulating an extraordinarily large antenna electronically by utilizing the platform's flight path. These sensors are active and do not rely on sunlight for imaging, as pointed out by Nie et al., (2022).Essentially, a SAR image is a 2D representation of the measured backscatter. It employs pulses of electromagnetic energy that can penetrate through clouds, smoke, and rain. This unique capability to penetrate through adverse weather conditions and low-light environments enables SAR to detect environmental changes.

SAR systems emit microwave signals and subsequently capture the reflected portion. They then use this information to calculate radar cross-section, providing a description of surface or reflective object (Tsokas et al., 2022). Since SAR functions as its own source of illumination, users can specify parameters like frequency, look angle, and polarization (Tsokas et al., 2022). The wavelength of the signal determines the depth of penetration, with lower frequencies or longer wavelengths allowing for greater penetration into materials like snow, vegetation, and alluvial structures (Tsokas et al., 2022).

Table 1 outlines microwave bands utilized by radar community, along with their corresponding frequencies and wavelengths. Among these bands, L, C, and X bands are the most employed in the SAR instruments. Choice of the look angle is primarily determined by the specific application and has a direct impact on the coverage width and resolution. Different polarization types exhibit distinct interactions with objects. Typically, SAR systems transmit and receive signals that are linearly polarized, either in a horizontal or vertical orientation. In the past, SAR instruments were limited to operating exclusively in either VV (vertical transmission and vertical reception) or HH (horizontal transmission and horizontal reception) polarization modes. However, modern SAR system has advanced to offer dual and quad polarization images, providing multiple perspectives of the observed scene. The utilization of quad polarization, also known as polarimetric SAR, allows the capture of a wide range of structural and textural information, facilitating identification of various scattering mechanisms. The specific combination of frequency, look angle, polarization, and illuminated area in a SAR dataset determines its suitability for specific applications (Tsokas et al., 2022).

Table 1: Designation of microwave bands (Flores-Anderson et al. 2019).

Band	Frequency	Wavelength	Typical application
Ka	27-40 GHZ	0.8-1.1cm	Airport surveillance (rarely used)
K	18-27 GHZ	1.1-1.7cm	H_2O absorption (rarely used)
Ku	12-18 GHZ	1.7-2.4cm	Satellite altimetry
X	8-12 GHZ	2.4-3.8cm	Urban monitoring, Ice, and snow (rarely used)
C	4-8 GHZ	3.8-7.5cm	Global mapping; Change detection; Monitoring of areas with low to moderate vegetation; Ice, ocean, maritime navigation (SAR workhorse).
L	1-2 GHZ	15-30cm	Geophysical monitoring, biomass and vegetation mapping.

2.2. Development of Radar Imaging Technology:

In the 1950s, during the initial phase of radar imaging technology, there was a growing interest in extracting geometric details from radar images. These radar systems operated with a side looking approach and made use of synthetic aperture method. These systems actively transmitted and received microwave pulses, resulting in the creation of images known as synthetic aperture radar (SAR) images. While SAR images resembled conventional grayscale optical images, the grayscale values were arranged based on Doppler effect in along-track direction and signal travel time in cross-track direction.

Since the first spaceborne SAR mission with SeaSat in 1978, numerous subsequent missions have been launched. These missions have produced a variety of SAR datasets, many of which are accessible to the public. Table 2 provides compilation of most widely recognized sources of SAR data from satellites that have already been launched or are planned for launch. Additionally, multiple airborne SAR missions have been and continue to be conducted in various countries worldwide. Measurements delivered by these SAR platforms find extensive application in a range of fields related to earth observation and object detection, as well as in advancement of new techniques. Most SAR sensors operate in multiple modes, each characterized by its specific polarization, resolution, and swath. Furthermore, SAR data come in diverse types and formats, and are made available at various processing levels.

Table 2. Satellite SAR missions (Tsokas et al., 2022)

Sensor	**Lifetime**	**Band (Wavelength)**	**Polarization**	**Agencies operating sensors**
Seasat	1978	L-band (24.6 cm)	HH	NASA (National Aeronautics and Space administration)
ERS-1	1991-2000	C-band (5.6 cm)	VV	ESA (European Space Agency)
JERS-2	1995-1998	L-band (24.6 cm)	HH	JAXA (Japan Aerospace Exploration Agency)
ERS-2	1995-2011	C-band (5.6 cm)	VV	ESA
ENVISAT	2002-2012	C-band (5.6 cm)	HH, VV, VV/HH, HH/HV, VV/VH	ESA

ALOS-1	2006-2011	L-band (24.6 cm)	Single, Dual, Full (dependent)	JAXA
Radarsat-1	1995-2013	C-band (5.6 cm)	HH	CSA (Canadian Space Agency)
TerraSAR-X;TanDEM-X	2007-; 2010-	X-band (3.5 cm)	Single, Dual Twin	DLR (German Aerospace Center)
Radarsat-2	2007-	C-band (5.6 cm)	Single, Dual, Twin	CSA
COSMO-SkyMed-2	2007-	X-band (3.5 cm)	Single, Dual	ASI (Italian Space Agnecy)
RISAT	2012-2017	C-band (5.6 cm)	Dual	ISRO (Indian Space Agency)
ALOS-2; PALSAR-2	2014-	L-band (24.6 cm)	Single, Dual, full (dependent)	JAXA
Sentinel-1	2014-	C-band (5.6 cm)	Single, Dual (dependent)	ESA
SMAP	2015	L-band (21.26 cm)	Full	NASA
Tiangong-2; InIRA	2016-2019	Ku-band (2.2 cm)	VV	CNSA (China National Space Administration)
Gaofen-3	2016-	C-band (5.6 cm)	Single, dual, Full (dependent)	CNSA
SAOCOM	2018-	L-band (24.6 cm)	Single, dual, Quad (dependent)	CONAE (Argentinian National Space Activities Commission)
PAZ SAR	2018-	X-band (3.5 cm)	Single, Dual, Twin	Hisdesat (Spanish satellite communications operator)
RCM (Radarsat constellation mission)	2019	C-band (5.6 cm)	Single, Dual, Compact, Full (dependent)	CSA
NISAR	2021	L-band (24.6 cm)	Single, Dual, Full	NASA

BIOMASS	2021	P-band (70.0 cm)	Full	ESA
SWOT; KaRIn	2021-	Ka-band (0.84 cm)	VV (right), HH (left)	NASA, CNES (French National Center for Space Studies), CSA and UKSA (United Kingdom Space Agency)
TanDEM-L	2023	L-band (24.6 cm)	Single, Dual, Full (dependent)	DLR

2.3. SAR: Basic principles and applications

SAR is an advanced radar system utilizing coherent microwave signals to illuminate specific targets or areas, generating detailed images of the scene. Despite the physical constraints of antenna size, SAR achieves significantly higher spatial resolution through a combination of antenna movement and a technique known as aperture synthesis. This involves creating a virtual antenna path alongside the actual antenna trajectory by integrating multiple measurements during movement. The movement direction of the antenna is termed as the azimuth direction, and SAR achieves resolution in this dimension through synthetic aperture processing, which separates reflections from distinct areas based on their Doppler frequency shift. The direction perpendicular to the movement is known as the range direction, where high resolution is achieved by accounting for the time delay of the reflected pulse. To prevent confusion between reflections originating from the same distance, SAR focuses exclusively on one side of the platform. Figure 2 provides a visual representation of the fundamental principles of SAR imaging geometry (Praks, 2012). Resulting SAR image serves as map, detailing spatial characteristics of target's reflective properties.

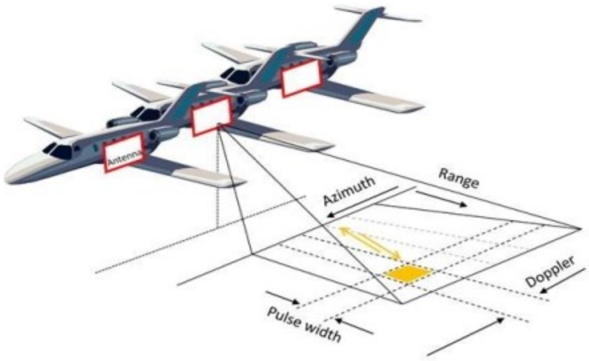

Figure 2. Synthetic Aperture Radar imaging geometry. (Praks, 2012)

2.4. Applications of SAR in Earth Observation

Initially, radar technology was primarily used for acquiring images independent of weather conditions and daytime. Over time, a diverse range of SAR techniques has been developed and is now applied in various fields. Recently, SAR technology has been employed in activities such as mapping, land classification, and various scientific disciplines including Geology, Glaciology, Wind studies, and Navigation.

SAR data have also been widely utilized in different earth observation applications including oceanography (Ye et al., 2016), glaciology, geography, and geology. In oceanography, SAR data provides detailed images of ocean surface features such as waves, wind, and currents. Unlike optical imaging, SAR is not affected by cloud cover or lighting conditions making it a reliable tool for accurate ocean surface monitoring.

SAR datasets, when combined with optimal remote sensing techniques, enable accurate monitoring of forest changes (Dyurgerov & Meier, 2000). Backscatter signal from soil and forest structure has been a subject of study for years (Ulaby et al., 1982). Additionally, SAR has been employed to monitor buildings and to assess damage in aftermath of earthquakes. Methods such as InSAR (interferometric Synthetic Aperture Radar) have been employed to analyze pre- and post-earthquake images, utilizing backscattering properties (Chen et al., 2016).Additionally, polarimetric characteristics (Park et al., 2013) and coherence-change have been investigated using an interferometric SAR coherence change technique with coherence filtering in both HH and HV polarizations. For instance, Watanabe et al., (2016) utilized this approach to identify damaged structures in areas affected by 2015 Gorkha earthquake. The affected parts of urban area were accurately identified by comparing coherence change values obtained before disaster (γ_{pre}) and during disaster (γ_{int}). Findings showed a significant reduction in coherence for numerous buildings in central Kathmandu that were destroyed completely, including temples in Durbar Square and Dharahara tower as shown in Figure 3.

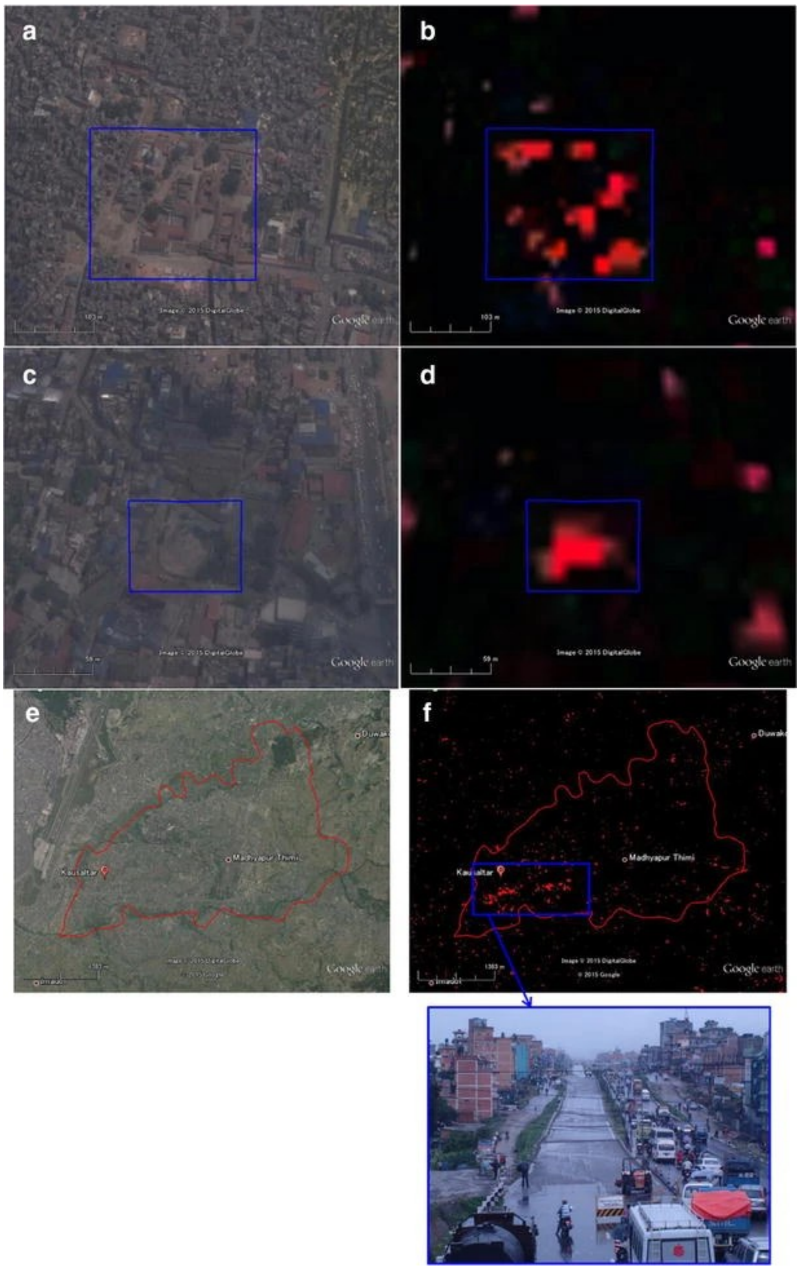

Figure 3.(a, b) Gangabu, (c, d) a mountainous area *(e, f) Kausaltar of Madhyapur Thimi* area. Left raw Google Earth image. Right raw Area with Δγ (HH, HV) ≥ 0.2, and coherence filter (Watanabe et al., 2016)

SAR data enables the retrieval of surface wind, wave, and current patterns in oceanic regions. Ocean waves create a distinctive pattern in SAR images, resulting from their rhythmic impact on local incidence angles and surface roughness (Romeiser, 2013). SAR technology offers high resolution imaging of ocean surface waves from space, free from the interference of cloud cover or variations in light conditions.

As time progressed, SAR datasets with varying polarizations became accessible. Converting HH polarized SAR date into VV polarized SAR data using a polarization ratio (Liu et al., 2013; Zhang et al., 2011) enables utilization of models. The Cross-polarized Normalized Radar Cross Section (NRCS) offers distinct advantages: it remains unaffected by radar incidence angle and wind directions, while maintaining a linear correlation with wind speed (Zheng et al., 2012). Moreover, it avoids issues related to saturation or ambiguity associated with high wind speed, (H. Shen et al., 2009), making it valuable for integrated approaches (Huang et al., 2017).

2.4.1.Soil Classification and Lithography

SAR is also pivotal in land classification. It helps in identifying and delineating specific soil types like laterites, silica sand and gold. In cases where purpose is to delineate specific soil compositions such as laterites (Da Silva et al., 2013), silica sand (Kausarian et al., 2017), or gold (Pedroso et al., 2014), the lithographic analysis can be reframed as a land classification issue. SAR data has proven to be useful in imaging structures of near-surface and delineating geological boundaries, as well as in categorizing sediments and mapping surfaces. Under specific conditions such as absence of vegetation and dryness SAR can penetrate to shallow depths in the subsurface. This capability allows SAR to identify geological features close to the surface or assist in lithographic analyses (Alban et al., 2018). Comprehensive workflow of their study can be seen in figure 4.

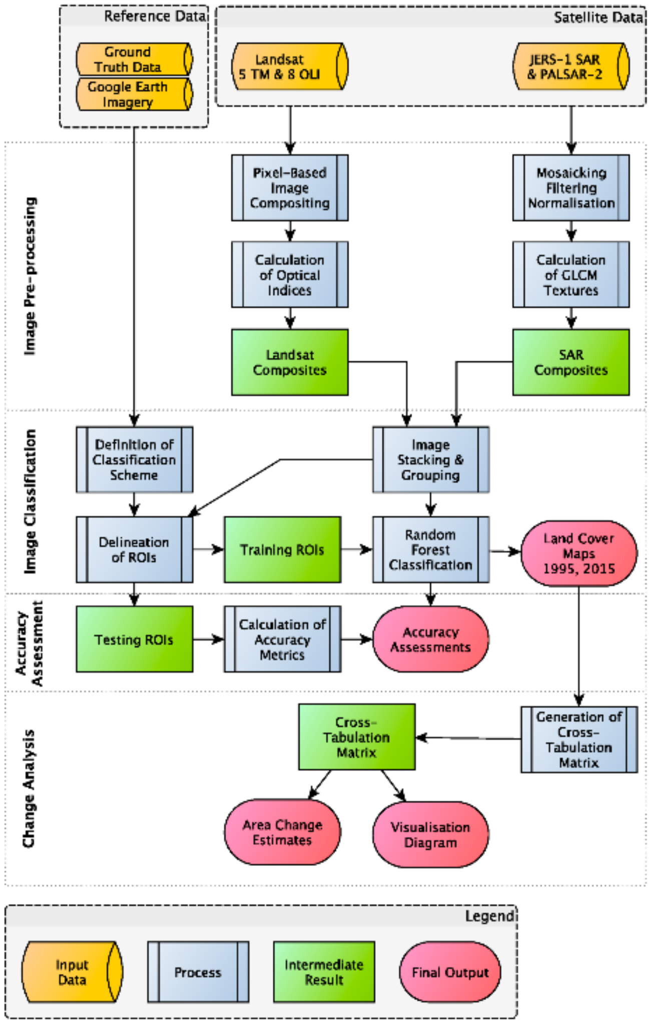

Figure 4. Workflow of land cover/use change mapping and analysis.(De Alban et al., 2018)

2.4.2. Geolocation and Calibration

SAR technology is also useful in accurate geolocation, which is vital for tasks like navigation and integration with geospatial data. This enables precise mapping and analysis of SAR images by providing accurate geographic coordinates. As SAR missions progressed, satellite providers recognized the crucial need for accurately assigning geographical coordinates to images. This facilitates rapid mapping and seamless integration with the additional geospatial data, such as road networks or optical imagery. Evaluation of the geolocation accuracy for SAR sensors, using ground truth coordinates of the features such as crossroads, stable Corner Reflectors (CRs), or active transponders, is an integral part of the geometric sensor calibration. This calibration process has been continuously updated and refined over lifespan of first-generation spaceborne SAR missions. Presently, typically it is carried out during the commissioning phase (Gisinger, 2020).

2.4.3. Oil Spill Detection

In environmental monitoring, SAR plays a crucial role in detection and classification of oil spills. By identifying dark formations on the sea surface, SAR helps in rapid response efforts and minimizing environmental impact. Discharge of oil from ships, whether accidental or intentional, has become an increasingly concerning issue due to the rise in maritime activity. Researchers have investigated how oil spills affect wind retrieval (Shen et al., 2019). In order to effectively monitor larger sea areas, satellite-based SAR proves to be a valuable tool (Singha et al., 2014). Oil spills typically create smooth patches on the sea surface, resulting in dark formations in SAR images. However, the detection process is complicated by other dark sea features, known as look-alikes. Process of the SAR oil spill detection involves three main steps (Topouzelis & Psyllos 2012): (1) identifying darker spots, (2) extracting object-based features, and (3) classifying them as oil spills.

2.4.4. Monitoring Soil Moisture

Efficient soil moisture monitoring is essential in preventing drought, optimizing irrigation systems, and ensuring sustainable agricultural practices. Polarimetric SAR provides a lot of information on soil moisture content which helps in agriculture as it provides a diverse set of data and has ability to penetrate through vegetation cover. The process of SAR based soil moisture retrieval comprises two key stages (He et al., 2014): (1) breaking down backscattering data into its components, (2) estimating soil surface parameters using inversion models. A thorough assessment was conducted to determine accuracy and sources of potential errors in this soil moisture retrieval method. Results, as depicted in Figure 5, demonstrated a strong correlation between measured and the estimated soil moisture levels (R2 = 0.71, RMSE = 3.32 vol.%, $p < 0.01$).

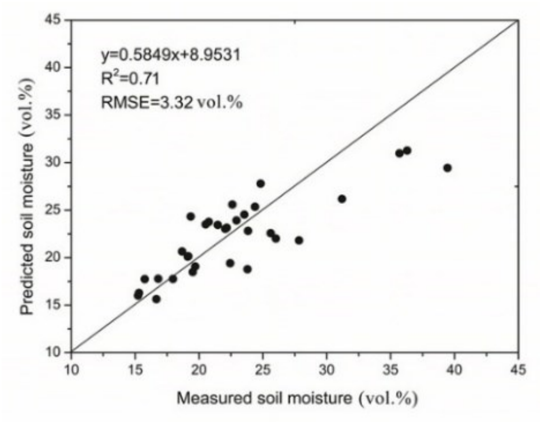

Figure 5. Correlations between measured and estimated soil moisture (He et al., 2014)

2.4.5. Object Detection

In the domain of security and defense, SAR is used for object detection and recognition. This ability is valuable in scenarios where visual imagery might be limited as SAR operates effectively in all types of weather conditions.Object detection, traditionally associated with computer vision and applied mainly to visual images, is also applicable to SAR imagery. SAR offers an advantage of providing images in adverse weather conditions and during nighttime. However, labeling SAR images for training purposes is more complex compared to visual images due to limited availability of large SAR datasets. Recent methods have addressed this challenge by integrating transfer learning from visual imagery into training process of SAR object detectors. (Rostami et al., 2019).

2.4.6. Military Applications

Detecting and identifying military vehicles such as aircraft and tanks are of significant military interest (Wang et al., 2016).Airport detection is of utmost importance due to its significant role in the economy and its potential as a military target. Automated airport detection also helps in airport operations including takeoff, landing and navigation. In SAR images, airports can be identified by delineating runways and taxiways from surrounding area (Chen et al., 2020).

2.4.7. SAR in Navigation

SAR data has also been employed in navigation. It provides absolute platform position information for both manned and autonomous aircraft, serving as an alternative component to GPS specifically in areas where GPS signals may be weak or unavailable. SAR technology is also being employed in providing precise platform position data for both piloted and autonomous aircraft, making it a valuable tool for geopositioning (Zhu et al., 2020). Odometry, on the other hand, monitors alterations in aircraft positions and orientation by observing distinctive ground reference points with onboard sensors. This process includes tracking landmarks in successive frames and computing inter-frame translation and rotation, which is a task with its own set of challenges (Wang et al., 2018).

2.4.8. Advancements in SAR coordinates Accuracy and Resolution

Significant work has been conducted on SAR coordinates accuracy, with notable studies for missions like ERS-1 (Werninghaus & Buckreuss 2010) and RADARSAT-1 (Chen et al., 2001). TerraSAR-X (Werninghaus & Buckreuss, 2009) and Cosmo SkyMed (Coletta et al., 2007) as upcoming SAR missions, have improved system accuracy and offer high resolution image products. They have been validated to provide three-dimensional positioning results within a range 0.5 to 1.5 meters for the natural features like streetlights and installed corner reflectors (Raggam et al., 2010); (Koppe et al., 2012) for TerraSAR-X and (Nitti et al., 2016)) for Cosmo SkyMed.

2.5. Comparison of SAR and optical data

2.5.1. In hazard monitoring and management

Satellite remote sensing is pivotal in all hazard monitoring and management stages (Capolongo et al., 2019). Traditional flood monitoring using remote sensing encounters challenges due to limited data availability with adequate acquisition frequency and timeliness (Shangguan et al., 2019). SAR offers a significant advantage in this context, as it operates reliably in both day and nighttime conditions (Shen et al., 2019). On the other hand, optical satellite systems capture rich information across various spectral bands, yielding favorable results in ground cover classification (Goffi et al., 2020). However, optical satellite images can be affected by unfavorable weather conditions, often leading to reduced quality during times of disaster characterized by cloud cover and rainfall (Li et al., 2018). In contrast, SAR images are impervious to weather conditions, making them the preferred choice during cloudy and rainy weather conditions. While SAR images primarily provide digital number values reflecting the backscatter characteristics of ground objects, this may pose challenges in ground cover classification due to limited information content (Huang and Jin, 2020). Nevertheless, SAR data can still sensitively detect changes in backscatter coefficients, offering valuable insights into variations in ground object properties and states. Particularly during flooding events, SAR backscatter coefficients tend to increase in all SAR bands over vegetated areas (Martinis et al., 2009).

2.5.2. In vegetation monitoring and mapping

In the field of vegetation mapping and monitoring, a range of remote sensing techniques utilizing different types of multispectral sensors have been successfully developed and applied over years (Luca et al., 2019; Grabska et al., 2019; Praticò et al., 2021). By utilizing spectral signatures that change over time in accordance with the phenological cycles of different seasons, it becomes possible to distinguish between different types of vegetation with greater accuracy, enabling their identification and characterization(Aragones et al., 2019; Grabska et al., 2020; Praticò et al., 2021; Solano et al., 2019).Grabska et al. (2019) employed a time series from Sentinel 2 to create a map of forest composition, illustrating effectiveness of seasonal phenology variations in enhancing spectral discrimination between species, achieving higher levels of accuracy compared to use of individual images. Moreover, spectral vegetation indices amplify sensitivity of single-band spectral signals to variability of biophysical states in plant tissues, photosynthetic activity, and leaf productivity (Aragones et al., 2019; Marzialetti et al., 2019; Praticò et al., 2021).

In addition to use of the multispectral data, several authors have explored applicability of active SAR systems for mapping land cover in tropical forests (Lapini et al., 2020; Nicolau et al., 2021). Apart from their operational capability in all conditions, these sensors offer diverse and supplementary physical data that augment spectral information when integrated with optical imagery (Nicolau et al., 2021; Spracklen et al., 2021). The total backscattered signal originating from forest vegetation arises from the combination and interaction of canopy and ground backscatters (Lapini et al., 2020). This reflected response is influenced by inherent sensor variables, such as wavelength and polarization, as well as characteristics of vegetation such as cover shape, structure and orientation, moisture level, and surface properties related to geometry and dielectric properties (Lapini et al., 2020).

2.5.3. In impervious surfaces estimation

Accurately estimating impervious surface area (ISA) poses challenges, particularly in subtropical humid areas where a diversity of impervious materials and cloud cover can be factors. Optical sensors for impervious surface estimation are often hindered by cloud cover, and this issue is exacerbated in humid regions. In contrast, SAR images are effective in humid conditions and function reliably in all weather conditions. However, SAR lacks the ability to capture as many spectral bands as possible, resulting in an overall lower accuracy in impervious surface estimation. To tackle these obstacles and deliver precise ISA estimations in areas like cloudy areas, H. Zhang et al., (2012) integrated both optical and microwave remote sensing. Their study aimed to conduct a thorough evaluation of these two data sources along with different techniques for ISA mapping. The classification outcomes and accuracy evaluation provided significant observations into differences between optical and microwave images. The comparison revealed that ISA estimation derived from ETM (Enhanced Thematic Mapper)+ images alone are more accurate than those obtained solely from ASAR images.

2.6. Challenges in using SAR data for Earth observation

In the past few years, significant progress has been made in development of Synthetic Aperture Radar (SAR) sensors, including the launch and enhancement of various systems such as GF-3, Cosmo-Skymed, X-SAR/SIR-C, ASAR/ENVISAT, ALOS/PALSAR, RADARSAT-2, Sentinel-1, Terra SAR-X, ALOS-2 multi-band, and satellites equipped with multi-polarization capabilities. A pioneering experiment focused on soil scattering, utilizing radar, revealed backscattering coefficients at specific frequencies within the X and dual-Ku bands. These findings were instrumental in calculating snow water equivalent in snowpacks (Xiong et al., 2021). Despite the numerous advantages of SAR remote sensing, a challenge lies in the reproducibility of results, warranting attention from researchers in the future (Balz et al., 2020).

Another challenge in SAR lies in the requirement for a high pulse repetition frequency to attain high resolution, which can cause a burden on the SAR system. Recent studies have put forward a design that creates numerous azimuthally virtual receiving apertures, offering a potential solution to this challenge (Shu et al., 2021).

SAR also faces problems related to geometric distortions that require precise correction during data retrieval from the satellite imagery. Notably, pixel size varies in both azimuth and range directions relative to satellite's orbit, resulting in different spatial resolutions. These discrepancies lead to different terrain effects that need appropriate handling (Javali et al., 2021).

Furthermore, SAR encounters the issue of speckle, a radiometric noise stemming from the non-uniform distribution of amplitude and phase. This phenomenon is primarily attributed to the roughness of the Earth's surface. Speckle leads to the prevalence of white spots in radar imagery, particularly in areas with transitions in land cover. It complicates the process of image interpretation and calls for the application of suitable filtering techniques. Addressing these challenges may involve advancements in the digital modulation domain to enhance spatial resolution (Genderen, 2016).

2.7. Solutions to overcome Geometric distortions and Speckle in SAR data

Yashi Zhou et.al., (2020) have introduced a high-resolution SAR system operating at 3.6GHz, utilizing full bandwidth for both airborne transmission and reception. While this approach enhances resolution, it also highlights motion related errors. To address this, they implemented a motion compensation (MOCO) technique, employing the differential global positioning system (DGPS) to improve the precision of inertial measurement equipment positioning. The team conducted a field experiment involving this very high-resolution SAR system and analyzed the results (Zhou et al., 2020).

Yahia et al. (2020) proposed a combined iterative filtering technique to address the challenge of speckle noise, a significant issue in Polarimetric SAR imaging radiometry attributed to echo recording. Unlike conventional methods based on variance, this technique utilizes coefficient variation to assess alterations in pixel values. It also incorporates anovel hyperbolic tangent and makes use of nonlocal neighborhoods for estimating related statistics. Through this approach, they effectively tackled the previously noted issue of diminished spatial resolution in multi-looking techniques (Yahia et al., 2020).

3. Corner reflectors

This chapter explains the role of corner reflectors in SAR's radiometric calibration, general criteria for designing the corner reflector and it's uses in geodetic SAR.

3.1. General criteria in designing a corner reflector

When designing corner reflector, several important considerations need to be considered. It should be easily adjustable for pointing, lightweight for easy transport, simple to mount, and secure from unauthorized access. Additionally, it should be sturdy enough to withstand various weather conditions. For validation experiments, the height of the reflector must be adjustable (Qin et al., 2013).

3.1.1. The Material of Corner Reflector

To ensure mechanical stability and accurate artificial shifts at a millimetric scale, it is recommended to minimize the size and weight of the corner reflector. For this purpose, aluminum is preferred material due to its low density and resistance to corrosion through passivation. On the other hand, Common iron have density ranges from 2.6g/cm3 - 2.9g/cm3 and for aluminium 7.75 - 8.05g/cm3, respectively. For instance, a small aluminum trihedral corner reflector measuring 50cm x 50cm x 75cm with a 2mm width weighs approximately 5.6kg (assuming a density of 2.8g/cm3). In contrast, if same corner reflector was made from steel, it would weigh 16kg (assuming a density of 8g/cm3), resulting in a significant increase in weight (Qin et al., 2013).

3.1.2. The Shape of corner reflector

Ideally, a corner reflector should exhibit much higher reflectivity compared to surrounding scatterers, implying high Radar Cross Section (RCS) for smaller size (Ferretti et al., 2007) Commonly used corner reflector shapes include flat plates, dihedrals, triangular trihedral, and square trihedral shown in figures 6(a,b,c). The respective RCS values for these shapes are detailed in Table 3 (Doerry et al., 2009). Notably, circular trihedral CRs offer an RCS like that of circular reflectors, but manufacturing square trihedral corner reflectors are generally more straightforward than circular ones.

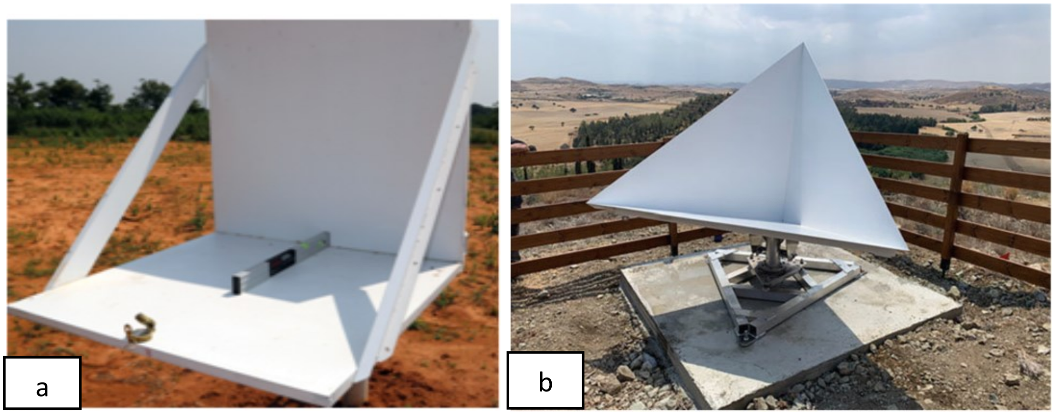

Figure 6(a). Dihedral Corner Reflector,(b). Triangular trihedral Corner Reflector

(c). Square Trihedral Corner Reflector (EOS_CAL_MicrowaveTargets | NRSC Web Site, 2015)

Table 3: RCSs of the most common reflectors (where a is the side length and λ is the wavelength) (Doerry et al., 2009)

Types of Reflectors	**Maximum RCS (m^2)**
Triangular Trihedral	$4\pi a^4/3\lambda^2$
Rectangular Dihedral	$8\pi a^4/\lambda^2$
Square Trihedral	$12\pi a^4/\lambda^2$
Circular (quarter disc) trihedral	$15.6\pi a^4/\lambda^2$

3.1.3. Installation of Corner reflectors

Corner reflectors play a crucial role in SAR imagery by providing distinct radar reflections with high intensity, ensuring a consistent signal to clutter (SCR) value over time. This allows for precise interferometric phase measurements with minimal variations and strong SCR values (Ferretti et al.,2007).

Selecting an appropriate site for corner reflectors is essential to minimize background backscattering. This can be accomplished by conducting a visual pre-analysis of SAR backscatter intensity images, which are obtained from level 1 single-look complex images provided by space agencies like ESA. These images assist in identifying areas with low background backscattering. Once the most suitable corner reflector test site is determined for each co-location, a corner reflector can be positioned on a mast for two or more SAR satellite passes (Parker et al., 2017).

Furthermore, it is imperative to orient the corner reflector in a manner that aligns azimuth and range of the boresight (originating from intersection of three triangular plates) vector with SAR satellite's line of sight. To maximize the Radar Cross Section (RCS), corner reflector should be installed on a horizontal plate. Direction of the reflectors should align with the line of sight to achieve the highest RCS, as demonstrated in Figure 7. Any deviation from this alignment or slight tilting may result in a decrease in RCS due to variations in the shape and size of corner reflectors.

Figure 7. Corner reflector of Metsähovi *is tilted* along Line of sight

3.2. Use of corner reflector in radiometric calibration of SAR

The performance of spaceborne synthetic aperture radar (SAR) can experience degradation over time due to factors like component wear, aging, and fluctuations in environmental temperature (Kirubanandam et al., 2019). To ensure optimal performance while in orbit, it's essential to address this degradation. This is achieved through a process called radiometric calibration, which establishes the relationship between the digital values recorded by the SAR and the corresponding backscattering coefficients (Kirubanandam et al., 2019). Ground-based corner reflectors (CR) play a crucial role in this calibration process. These passive devices are designed to effectively reflect radio waves back towards their source. As such, they serve as valuable tools for calibrating radar systems(Shu, 2017). Corner reflectors are strategically placed in locations that enable them to bounce radar signals back to the satellite from specific positions. They are particularly useful for acquiring displacement measurements in areas densely covered by vegetation or snow. Trihedral radar reflectors, often referred to as corner reflectors, derive their name from their three mutually perpendicular plates. This configuration, resembling a corner of a cube, consists of one baseplate and two vertical plates, ensuring efficient reflection of radar waves (Garthwaite et al., 2015).

Triangular trihedral CR (shown in figure 8) have been used for many years in calibrating SAR images. These have also gained widespread recognition as effective tools for accurate measurement of ground deformation using InSAR techniques (Garthwaite et al., 2015).

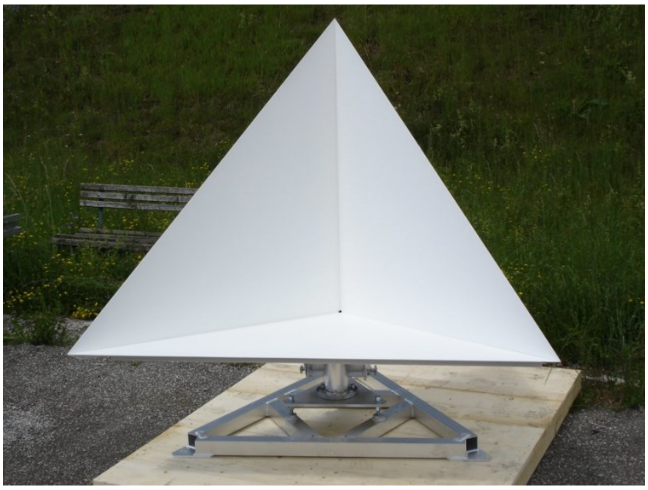

Figure 8. Triangular Trihedral Corner Reflector (Döring et al., 2007)

3.3. Use of corner reflectors in Geodetic SAR

Corner reflectors which are a key component of SAR technology play a very important role in enhancing the precision and reliability of geodetic SAR applications. These reflectors are strategically positioned within the terrain to facilitate accurate measurements over time. By effectively addressing challenges related to temporal and geometric distortions, corner reflectors significantly enhance the performance of SAR techniques. Corner reflectors have also proven valuable as reference points in extended time series of interferometric SAR images (Xia et al., 2002). In monitoring landslides in the Three Gorges area of China, efficient corner reflectors have been employed in SAR applications to mitigate potential fluctuations in ground surface reflectivity, thereby preserving the accuracy of SAR measurements (Ye et al., 2004).

3.3.1. Use of corner reflectors for Ground Deformations and Target Detection

The use of CRs in Differential Interferometry Synthetic Aperture Radar (DInSAR) technique presents a promising advancement in overcoming limitations seen in conventional DInSAR for ground deformation monitoring. While DInSAR shows potential for accurate measurements, it is susceptible to challenges related to temporal and geometric decorrelation (Fu et al., 2010). To tackle this Bovenga et al., (2012) integrated corner reflectors as passive reflectors within a multi-temporal differential SAR interferometric analysis, proving especially valuable in areas characterized by complex terrain and variable vegetation cover. Additionally, Stastny et al. (2014) also utilized radar corner reflectors to detect small vessels in SAR data. Moreover, there's a proposal to deploy a network of corner reflectors in areas lacking coherent targets for monitoring, particularly in challenging terrains using SAR, for enhanced capabilities (Bovenga et al., 2014). Furthermore, studies on the analysis and scattering behavior of dihedral corner reflectors in bistatic SAR have contributed to optimizing bistatic radar systems, particularly in scenarios involving stealth targets (Ao et al., 2017).

3.3.2. Advances in SAR positioning and SCR estimation with corner reflectors

Gisinger et al., (2017) investigated differential positioning using TerraSAR-X in SAR applications. They explored the limitations of conventional corner reflectors, considering factors like intersection geometry, atmospheric corrections, biases, and observation noise. Study primarily focused on SAR reflector properties and developed a differential positioning method.

Experiment confirmed viability of differential approach for short distances without doing external corrections. This highlighted advantages of employing multi-directional reflectors in conjunction with the high-resolution TerraSAR-X data. The achieved 3-D positioning accuracy of 2-3 cm demonstrates potential benefits of such configurations in SAR positioning. Additionally, comparative analysis of the TerraSAR-X and Sentinel-1, emphasizing geolocation accuracy and observation quality, was conducted by Gisinger et al.,(2021). The accuracy of TerraSAR-X products was validated using different SAR modes and corner reflectors. This research effectively rectified geometric distortion in Sentinel-1 results using post-processing corrections based on SAR theory. It further demonstrated the potential for combining data from both missions through joint analysis of corner reflector reference coordinates, providing valuable insights for SAR applications. Corner reflectors have also found applications is estimating signal to clutter ratio in SAR interferometry and positioning. By utilizing time series of SAR measurements and assuming temporal uniformity, the proposed methods offered a more realistic and accurate estimation of SCR compared to traditional spatial methods (Czikhardt et al., 2022). Additionally, active radar transponders along with SAR have also been employed to observe sea level height in the Baltic Sea (Gruber et al., 2022).

4. Materials

This chapter gives details about the selection of research sites, comparison of corner reflectors at these locations and determination of their precise positioning. It also provides an in-depth explanation of the tools and methods which were employed to process and analyze gathered data.

4.1. Study Sites

Two primary sites i.e., Loviisa and Metsähovi were chosen for the comparative analysis of their respective corner reflectors. Loviisa is located on southern coast of Finland in Uusima region. Corner reflector at Loviisa was installed within 20 meters of the GNSS station, a critical tool for geodetic and navigation purposes. The CR was installed in December 2021, with inner leg length 1.5 meters and a triangular trihedral design with an opening angle of over 40 degrees.

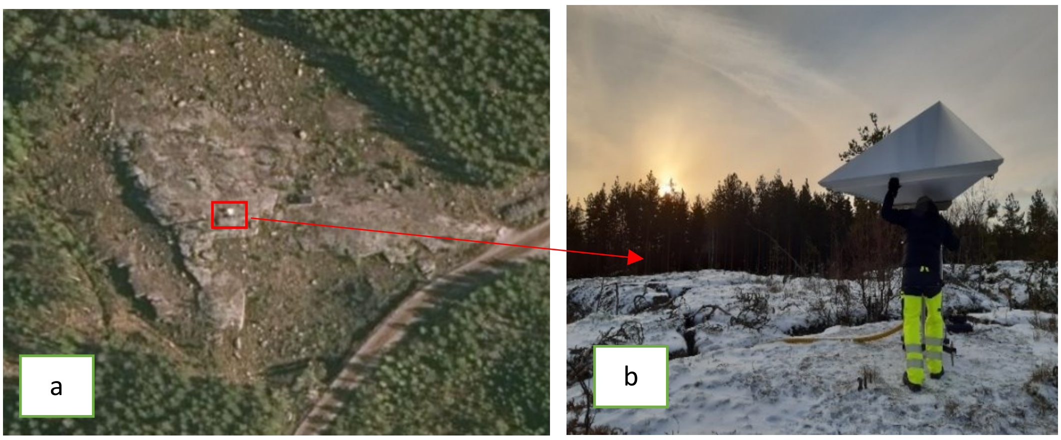

Figure 9. (a) Aerial view of CR at Loviisa site (b)Corner reflector installed at Loviisa site.

The other corner reflector is situated in Metsähovi, a geodetic and an astronomical observatory located in the municipality of Kirkkonummi, Southern Finland. The first corner reflector in Metsähovi was installed in 2013 and two additional ones were recently added in 2023. For this study, the efficiency of the corner reflector from 2013 was investigated. It shares similar properties with Loviisa's corner reflector, featuring a 1.5-meter inner leg length and an opening angle of over 40 degrees.

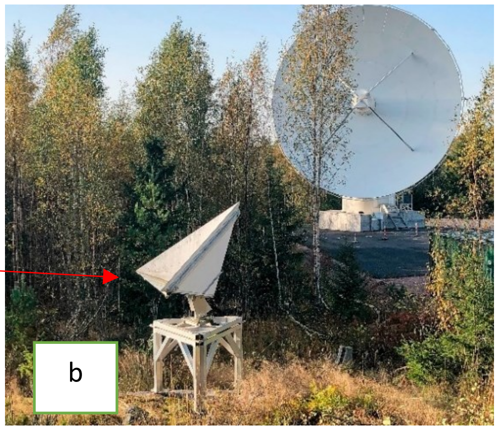

Figure 10. (a) Aerial view of Metsähovi (b) Corner reflector installed at Metsähovi station

4.2. Data acquisition

4.2.1. SAR data

SAR imagery was utilized to compare the efficiency of corner reflectors. These images offer the advantage of being accessible regardless of weather conditions and are typically displayed in grayscale where varying shades indicate differences in radar backscatter intensity. Darker areas represent lower backscatter, while brighter areas denote higher backscatter. These SAR images were obtained from Copernicus hub (https://scihub.copernicus.eu/dhus/) an initiative by the European Union for Earth observation and environmental monitoring. It provides free access to data collected by Copernicus Sentinel satellites and other contributing missions. These SAR imageries were then processed using SARPROZ software to visualize the corner reflectors in SAR.

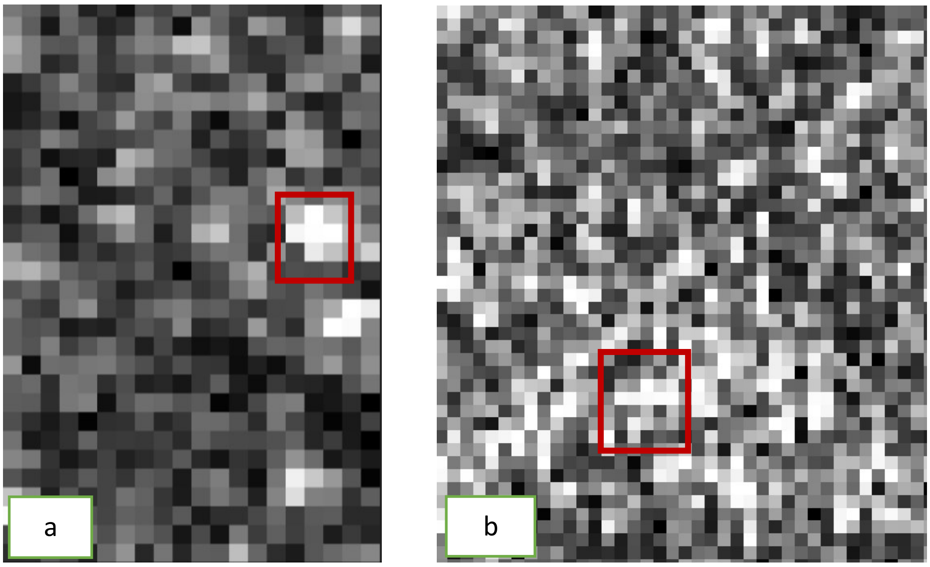

Figure 11. (a)Corner reflector of Metsähovi in SAR imagery (b) Corner reflector of Loviisa in SAR imagery

4.2.2. Weather Data

Snow depth and temperature data were sourced from Metsähovi's weather station for Metsähovi's corner reflector and from Finnish meteorological institute's Open Access Data (https://en.ilmatieteenlaitos.fi /download-observations) for Loviisa site.

4.3. Methodology

To assess and compare the effectiveness of the corner reflectors, Signal to Clutter ratio (SCR) values were computed using the Point Target Analysis (PTA) software provided by TUM (Gisinger et al., 2021) . This software facilitates the retrieval, processing, and generation of SCR data from SAR images. The SCR values were subsequently compared with two variables: snow depth and temperature, to understand how snow conditions impact the performance of corner reflectors.

The following steps outline the process of locating corner reflectors and deriving SCR values from SAR images:

4.3.1. Point Target Analysis

Within SAR image processing, accurately pinpointing the corner reflector holds a pivotal importance in the PTA process. PTA provides precise measurements of range time and azimuth, along with valuable data such as signal to clutter ratio values. From theoretical point of view, precise range and azimuth coordinates of a CR can be determined with remarkable accuracy, down to less than 1/100th of a pixel. This level of precision is primarily influenced by SCR values of point response.

Because of finite bandwidth of transmitter and restricted duration of interaction between radar beam and the ground, SAR signal is inherently constrained in both range and azimuth. As a result, the point response of a corner reflector is distributed across multiple pixels in the image. This dispersion manifests as a characteristic cross-shaped signature, as shown in Figure 12.

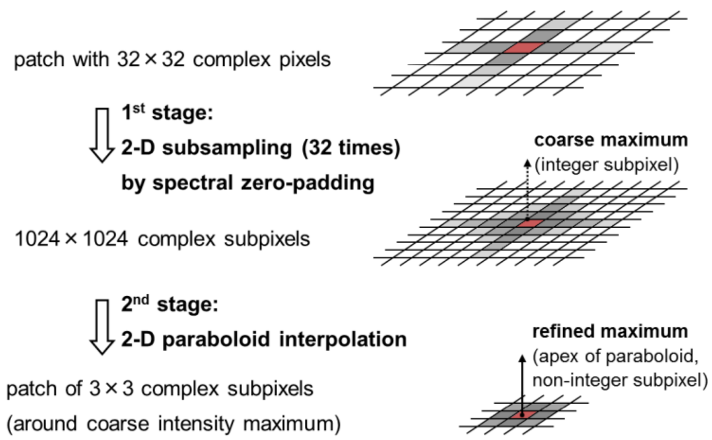

Figure 12. Schematic of the two-step procedure used to extract the peak of the CR response from a SAR single look complex(SLC) image. (Gisinger et al., 2021)

4.3.1.1. Oversampling

Oversampling is a crucial technique employed to enhance the precision of data extraction. Practically, to achieve a highly precise extraction, a technique called spectral zero-padding has been used. This technique involves supplementing the spectral representation of the analyzed patch with additional data points. Specifically, a 32x32 pixel area having the CR point response was oversampled to facilitate accurate analysis.

The oversampling process was achieved by expanding 2-D spectrum, computed through Fast Fourier Transform, with extra zeros at spectral minimum. This substantially enhances the level of detail captured in data, aiding in precise localization of peak. However, employing excessively large number of zeros, such as 1024 or 2048, can present challenges. While it offers a high degree of over sampling, it comes at the cost of increased memory usage and slower computational speed.

To strike a balance between precision and efficiency, a more effective approach involves a combination of zero-padding using factors of 32 or 64, along with refinement process employing an analytical surface have been found. This integrated method allows for the maintenance of a satisfactory level of accuracy in peak detection, while mitigating the resource- intensive aspects associated with extreme oversampling. It serves as a practical and efficient means to address the challenges encountered while working with extensive datasets in research.

4.3.1.2. Fitting elliptic paraboloid shape

According to Gisinger et al., (2021). Fitting an elliptical paraboloid shape serves as a critical component in the Point Target Analysis (PTA) approach. This mathematical model accurately describes the shape of the analyzed data. The model is defined by the equation:

$$f(i,j) = a_0 + a_1(i - m_i)^2 + a_2\left(j - m_j\right)^2 + a_3(i - m_j)(j - m_j) \qquad 1$$

Here, i and j denote the indices of the pixels, while a_0, a_1, a_2, a_3 are the coefficients that define the shape of the paraboloid. Additionally, m_i and m_j represents the refined pixel positions of the peak location. To apply this model, emphasis was placed on the central 3x3 pixels region surrounding the peak in the amplitude image, as illustrated in Figure 4.14. This region provides the most relevant data for accurately characterizing the shape. After extensive testing, where the effectiveness of high zero-padding factors was compared to a two-step approach, it was observed that the latter method consistently maintained the required level of precision. This approach achieved accuracy levels better than 1/100th of a pixel.

4.3.2. Positioning of the Corner reflectors

Following calculation of SCR values, subsequent step involved accurately determining positions of corner reflectors. For this, applying corrections for both atmospheric delay and geodynamic influences are needed.

4.3.2.1. Atmospheric corrections for corner reflectors positioning

Electromagnetic waves passing through Earth's atmosphere experience a reduced group velocity in comparison to the speed of light in a vacuum. This results in a group delay for SAR signals travelling through the atmosphere. Consequently, if speed of light in a vacuum is assumed to convert measured two-way travel time to geometric range, the resulting SAR ranges become excessively large (Gisinger et al., 2021). Space geodetic techniques such as GNSS utilize radio signals and methods have been developed to determine and rectify atmospheric delays. These methods reveal that atmosphere can be divided into two components for radio signals up to 30 GHz. First is a non-dispersive neutral portion known as the troposphere and other is a dispersive part consisting of free electrons and ions referred to as ionosphere. Typical impact of tropospheric delay on the SAR slant range is in range of 2.5-4 meters, while ionospheric delay may reach several decimeters for X-band (9.65 GHz, TerraSAR-X) and several meters for L-band (1.2 GHz, ALOS-2).

4.3.2.2. Geodynamic corrections for corner reflectors positioning

Geodetic measurements including those obtained from SAR satellites are influenced by the dynamic behavior of Earth's solid crust. To precisely establish the reference position of a corner reflector, state of Earth's crust should be modeled to describe CR's reference position at the time of the SAR acquisition. For Sentinel-1, precise orbit determination was facilitated by onboard GNSS systems, aligning with International Terrestrial Reference Frame (ITRF). This alignment enables use of ITRF conventions for corner reflector positioning modeling. The ITRF as defined by International Earth Rotation Reference System Services (IERS), incorporates various crustal displacements related to tidal dynamics. The table 4 provides a comprehensive list of all considered effects, along with their typical magnitudes. The primary contributor is direct tides of solid Earth, causing variations of daily position in centimeters horizontally and decimeters vertically.

Table 4: Order of the magnitude of solid Earth effects that must be considered when modelling CR coordinates in ITRF as given by IERS conventions.

Solid Earth Effect	**Horizontal(mm)**	**Vertical(mm)**
Solid Earth tides	± 50	± 200
Ocean tidal loading	±10	±50
Atmospheric tidal loading	±1.5	±6
Ocean pole tide loading	±0.2	±1.5
Secular trends(tectonics) up to	100mm/y	15mm/y

Furthermore, secondary effects originating from ocean and atmospheric tidal loading, as well as rotational deformations associated with polar motions, are addressed in accordance with IERS conventions (Gisinger et al., 2021). This framework enables the precise definition of the instantaneous corner reflector position:

$$X_{CR}(t_{SAR}) = X_{CR}(t_{CR}) + \dot{X}_{CR}.(t_{SAR} - t_{CR}) + \Delta X(t_{SAR}) \qquad 2$$

In equation 2 $X_{CR}(t_{CR})$ represents tide free ITRF position vector of CR determined by the terrestrial survey at an ITRF epoch t_{CR}. $\dot{X}_{CR}$ denotes linear displacement (tectonics) of CR site in ITRF, t_{SAR} corresponds to epoch of SAR observation and $\Delta X(t_{SAR})$ encompasses all periodic models of solid Earth displacement evaluated during SAR observation period.

Following implementations of these corrections, reference coordinates were then fed into the software, which subsequently generated the positioning coordinates of the corner reflectors. Additionally, it produced residual error graphs, as well as North-East and Height-East error graphs, explaining the differences or positioning offset in East, North direction, and Height.

5. Results

This chapter shows a comprehensive analysis of the data obtained from the study conducted at Metsähovi and Loviisa. The analysis was carried out for SCR and snow depth for both location's corner reflectors as well as temperature variations, residual errors, and ellipsoidal errors (North-East and Height- East) for both locations.

5.1. Objective 1: Impact of snow depth on SCR

As the first objective was to understand how snow affects the SCR of corner reflectors, here the SCR plots obtained using point target analysis software provided by Technical University Munich are analyzed using snow depth and temperature information obtained from the weather stations. Results were divided into two parts: Metsähovi and Loviisa. As observation period was September 1, 2022, to June 26, 2023, the effect of winter and thus, snow can be seen in results.

5.1.1. Metsähovi

Figure 13 shows a combined plot of SCR values in decibels (left y axis) and snow depth in centimeters (right y axis) for Metsähovi's corner reflector. The SCR values vary between 5 and 20 dB, expected values for SCR should be higher than 20 dB to show that corner reflectors are working efficiently. In late November snow starts to accumulate reaching maximum depth of 40cm by mid- December. It can be clearly seen that as snow depth increase SCR values start to show unstable behavior. With every peak in the snow depth there exists a dip in SCR values graph.

The temperature variations of Metsähovi are shown in Figure 14. The daily variability between night and day can be seen clearly, as well as the temperature change from autumn to winter and to spring. By comparing SCR, snow depth and temperature variations value among each other effect of efficiency of corner reflector with varying temperature and snow accumulation can be understood.

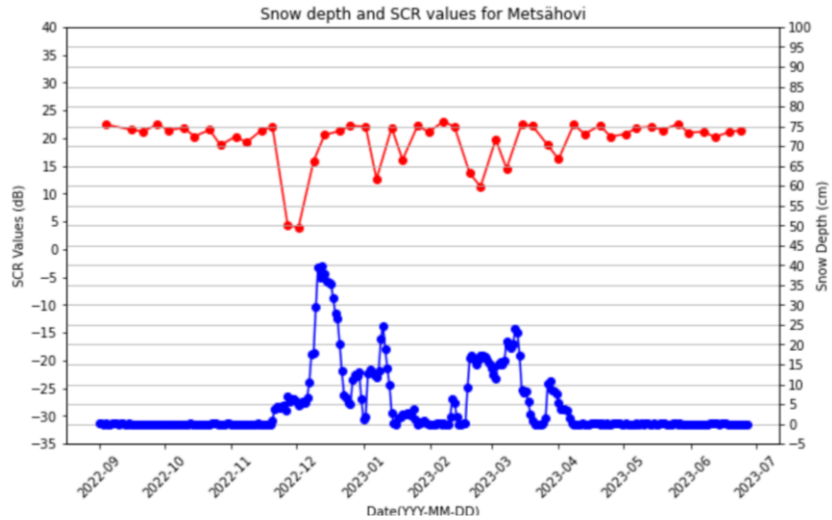

Figure 13. Snow depth and SCR values for Metsähovi site

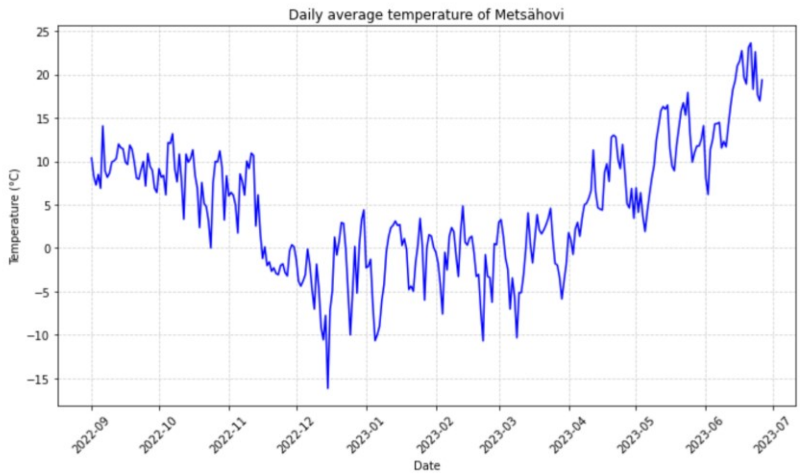

Figure 14.Daily average temperature of Metsähovi

5.1.2. Loviisa

Figure 15 shows combined plot of SCR values and snow depth, with SCR values represented on left y axis and the snow depth on right y-axis. In case of Loviisa, the SCR values vary between 0 and 20 dB. The graph demonstrates a noticeable trend in SCR values, exhibiting fluctuations in response to changes in snow depth. Specifically, during periods of increased snow accumulation, there appears to be a corresponding trend of variance in SCR values. Noticeable event occurred during mid-January where snow depth value is 54cm SCR value of CR started decreasing and dipped down to 0dB. After that with the varying snow depth values fluctuations can also be observed in SVR values till early April. This suggests a potential relationship between snow accumulation and the SCR values in this context.

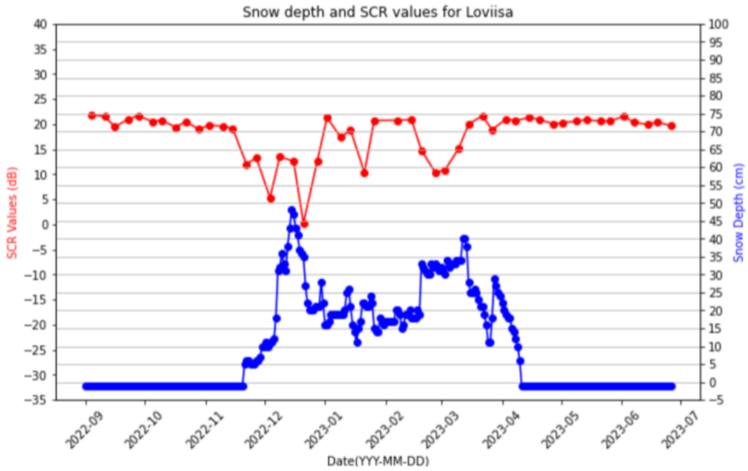

Figure 15. Snow depth and SCR values for Loviisa

Similarly, in Loviisa, a parallel examination of the temperature variations for the same time was conducted. Figure 16 shows the changes in temperature. By Examining temperature variations and snow depth alongside SCR values, a more comprehensive understanding of how environmental factors interact to influence the performance of corner reflectors was gained.

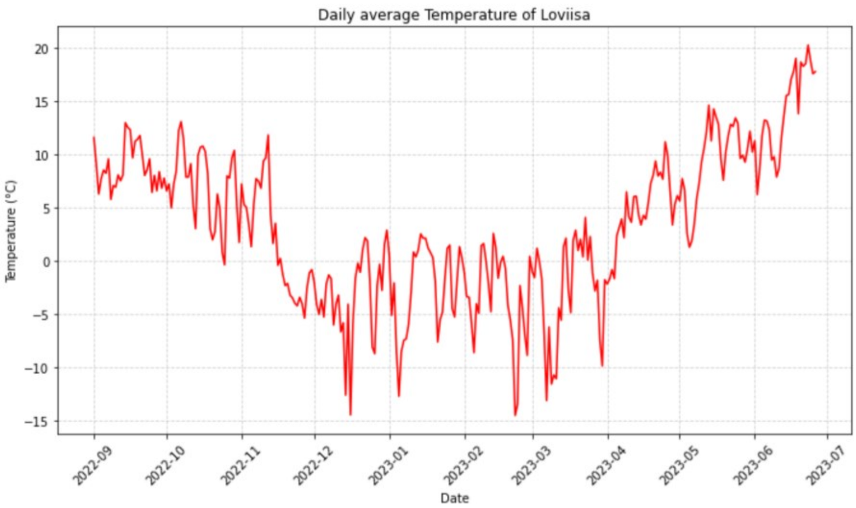

Figure 16. Daily average temperature of Loviisa

5.2. Objective 2: Positioning results of Metsähovi VS Loviisa

The second objective was locating precise position of the Corner Reflectors to compare their efficiency and performance in SAR imagery . The determination of CR'S position is also important in comprehending its behavior, as positioning relies on SCR values. For this purpose, ITRF reference coordinates were given to the PTA software which after performing necessary corrections gave positioning results in ITRF coordinate system and displayed residual analysis graph which helped in better understanding the accuracy of the results. In residual analysis graph, residuals are on y axis in m and time is on x axis. This software also displayed ellipsoidal error analysis North-East(horizontal plane) and Height-East(vertical plane) graphs. The NE error analysis graph gave difference in positioning from the reference coordinates, and HE error analysis graph provided offsets in Height and North direction. These ellipsoidal accuracy graphs showed the accuracy of the results.

5.2.1. Residual Error Analysis for Metsähovi

To make sure that the corner reflector at Metsähovi is in the right spot, reference coordinates which were given to the software and after calculations, coordinates obtained from the software are given in table 5 which show that the actual position was little different. Figure 17 shows residual graph indicating outliers in positioning. Different colors and show Range and Azimuth and different symbols show different swaths of Sentinel 1 i.e., ◊ symbol shows 34° and ○ symbol shows 41 ° swath angle. In case of Metsähovi the range observations seem to be more stable showing one peak which went beyond 0.5 m and residual values are between 0 and -0.5.

Table 5: Reference and Resultant coordinates of Metsähovi in ITRF 2014.

Cartesian coordinates	Reference coordinates(m)	Resulting Coordinates(m)
X	2892592.4652	2892591.0983
Y	1311867.9661	1311869.4818
Z	5512592.9985	5512592.1300

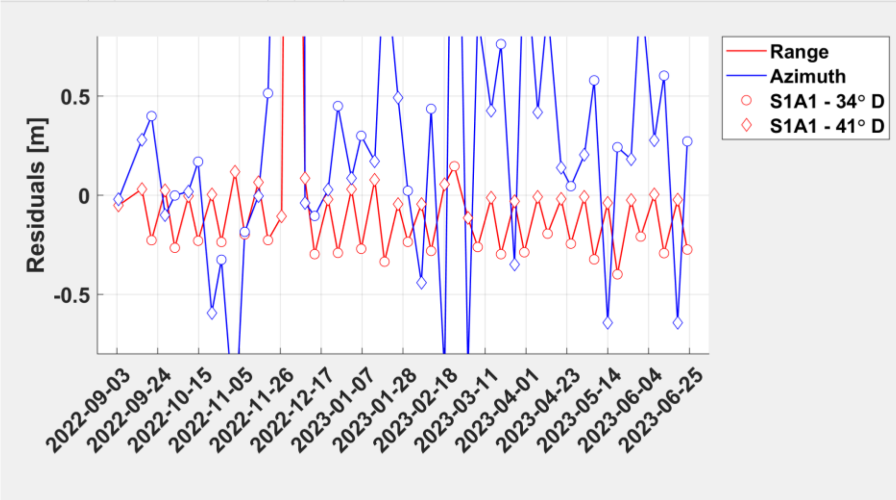

Figure 17. Residual error graph for Metsähovi

5.2.2. Ellipsoidal Error Analysis (NE and HE) for Metsähovi

Figure 18(a) illustrates any offsets in positioning in the vertical plane, i.e., HE. Figure 18(b) depicts the measurement of uncertainty in positioning in horizontal plane i.e., NE. In this representation, the exact positioning of the corner reflector is indicated with a red triangle symbol. These graphs help in seeing if there are any correlation or gross errors in positioning.

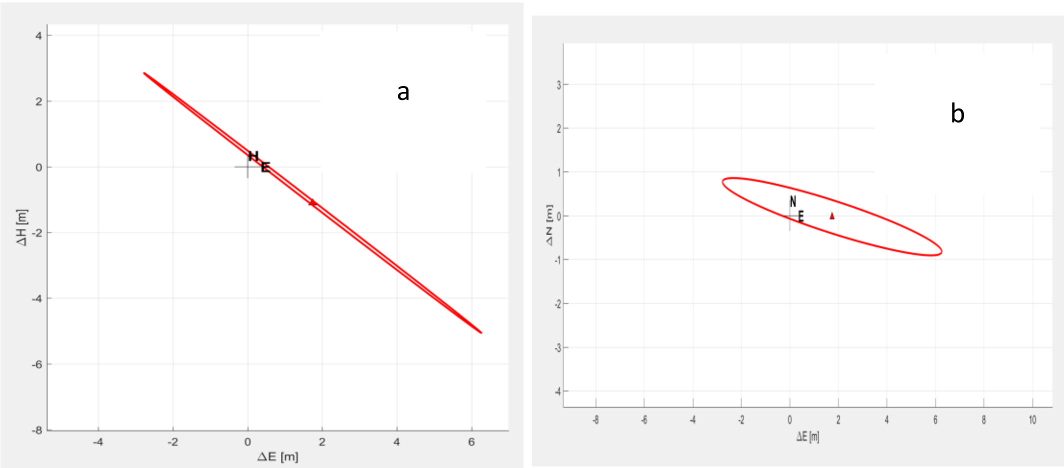

Figure 18. (a) HE ellipsoidal error graph for Metsähovi (b) NE ellipsoidal error graph for Metsähovi

5.2.3. Residual Error Analysis for Loviisa

To ensure the accurate position of the corner reflector at Loviisa, reference coordinates in ITRF system was established and fetched to the software which then generated exact positioning coordinates of CR which are given in table 6. Figure 19 shows that this adjustment is minor and ensures precise placement. In this figure, red line indicates Range and blue indicates Azimuth. Different swaths of Sentinel 1 are indicated by different symbols such that ◊ symbol shows 35° and ○ symbol shows 42 ° swath angle. In case of Loviisa, one peak can be observed in range residuals in late November other than that all other residual values of range are stable and are between 0 to -0.1m. Whereas, residuals for Azimuth are highly unstable showing larger residuals i.e., more than 0.5m.

Table 6: Reference and resultant coordinates of Loviisa in ITRF 2014.

Cartesian coordinates	Reference coordinates(m)	Resulting Coordinates(m)
X	2828356.8805	2828356.2746
Y	1396894.0839	1396893.1745
Z	5524908. 4065	5524907.5983

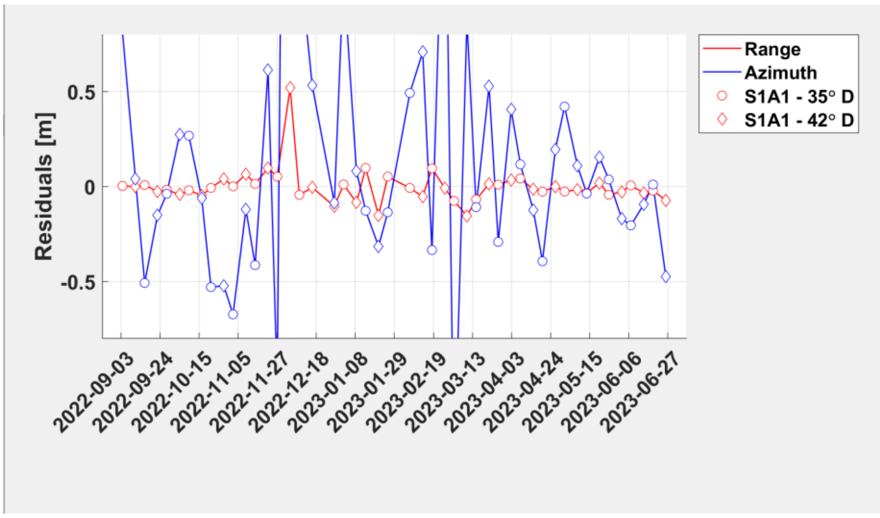

Figure 19. Residual error graph for Loviisa

5.2.4. Ellipsoidal Error Analysis (NE and HE) for Loviisa

Additionally, ellispoidal analysis (NE and HE) graphs were also generated to assess the accuracy of the positioning. Figure 20(a) illustartes any offsets in vertical plane, while figure 20 (b) displays difference between reference and exact coordinates. Exact coordinates obtained through TUM program is displayed with red triangle showing a difference of -0.5 with the reference coordinates.

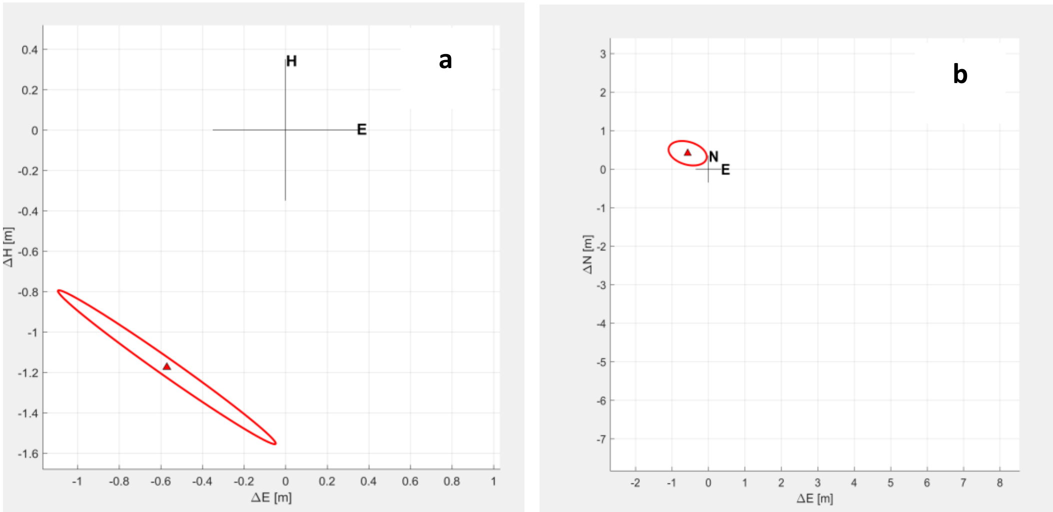

Figure 20. (a) HE ellipsoidal error for Loviisa (b) NE ellipsoidal error for Loviisa

6. Discussions

This chapter explains findings of the study, focusing on the impact of snow accumulation and temperature variations on the efficiency of the corner reflectors at Metsähovi and Loviisa. Additionally, it also addresses the accuracy of the positioning of these reflectors.

6.1. Objective 1: Impact of snow on SCR values

In the study conducted by Schiller et al., (2023) a comprehensive examination of the corner reflectors situated at Metsähovi and Loviisa was performed and a comparative analysis with Swedish corner reflectors was also done. The present research is an extension of their investigation, focusing on the impact of snow accumulation and temperature variations on the efficiency of the corner reflectors at Loviisa and Metsähovi alongwith their positioning. Notably, Metsähovi's corner reflector, having been operational for a decade and exhibiting a consistent efficiency, can serve as a reliable benchmark for corner reflector of Loviisa.

Related to impact of snow on SCR value, before testing and comparing SCR values with snow accumulation and temperature variations, it was assumed that snow has a degrading effect on SCR values and with the rise in temperatures snow will melt which can improve the SCR values.

In Figure 13, it was observed that Metsähovi's Corner Reflector (CR) consistently displayed higher signal to clutter ratio (SCR) values, exceeding 20dB from early September 2022 to mid-November. This period coincided with a lack of snow, with only a slight dip in mid-October to around 15dB. This indicates that the corner reflector effectively reflects a substantial amount of radiowaves. Around November 18th, there was a sudden drop in SCR values, reaching approximately 5 dB. This aligns with the first recorded snowfall, confirmed by the rise in snow depth values. By closely observing the snow depth and SCR values graph in late December it can be noticed that the snow depth values appear to be significantly high i.e., approximately 15cm. But surprisingly the CR exhibited higher SCR values. But looking at the temperature shown in figure 15 it was observed that for that period temperature is still in negative which means that snow did not melt away and is still on the ground. One possible reason for this anomaly could be that at Metsähovi during snow season, CR has been cleared at random intervals. It is reasonable to assume that during this time, the CR was cleaned even though there was still a substantial amount of snow on the ground, leading to the observed higher SCR values. Overall, as snow depth reached its highest point on the graph, a corresponding decrease in SCR values can be observed. This clearly illustrates how snow significantly affects the reflector's performance.

In Figure 14, we can see how snow affects Loviisa's corner reflector (CR). Overall, CR is working efficiently which can be predicted by looking at SCR values which it exhibited. But it can also be noticed that snow has an impact, causing some ups and downs in SCR values during winter. One interesting event can be seen in early April. Usually, with more snow, it is expected that the CR will work less effectively. But here, it is the opposite. The CR has been unattended since it was installed, so it was not cleaned manually from snow during this time. Figure 16 helps in explaining this it shows the temperature in Loviisa. By looking closely at the temperature graph for early April, temperature slowly went up from around -9 degrees Celsius to 0, and then kept going up. This means that as the temperature increased, the snow on the CR naturally started to melt. Also, it is worth noting that the last day it snowed was on 27 March, so the snow in April was already there which means snow depth values are of the older snow and melted as the temperature rose.

To conclude, it has been observed that our assumption about effect of the snow accumulation on SCR values turned out to be true.

6.2. Objective 2: Metsähovi VS Loviisa

Exact positions of the corner reflectors at Metsähovi and Loviisa were also determined. The accuracy of the positioning was within 1.9 meters for Metsähovi and very close, within -0.6 meters, for Loviisa. This information is shown in Figures 18(b) and 20(b), where the triangle symbol (△) represents difference between known reference coordinates and actual obtained coordinates. The red ellipsoid indicates the area within which the corner reflector can be located. Figures 17 and 19 show residual error graphs showing range and azimuth values on two different swaths which are steeper and flattening angles, respectively. These residual graphs can help in indicating during which period abnormalities occur.

Minimum residual error values result in getting highly precise positioning such that in case of Metsähovi the residual error is between 0 and -0.5 except for late November where an outlier occurred. For Loviisa, this residual error is nearer to 0 only except for early December where it went till 0.5. This could be explained by a drop in the signal strength, which we observed in Figure 14. This signal strength directly affects the positioning accuracy.

(Schiller et al., 2023) also determined the precise positions of the corner reflectors at Metsähovi and Loviisa. While their findings align closely with our results, there exists some difference in coordinates. These differences can be due to anomalies in late November for Metsähovi and early December for Loviisa. The comparison of coordinate values can be found in tables 7 and 8 below:

Table 7: Schiller's and our measured coordinates of Metsähovi in ITRF (2014)

Cartesian coordinates	Schiller's coordinates(m)	Our measured coordinates(m)
X	2892592.3127	2892591.0983
Y	1311868.2060	1311869.4818
Z	5512593.1975	5512592.1300

Table 8: Schiller's and our measured coordinates of Loviisa in ITRF (2014)

Cartesian coordinates	Schiller's coordinates(m)	Our measured coordinates(m)
X	2828356.1916	2828356.2746
Y	1396893.3833	1396893.1745
Z	5524907.3823	5524907.5983

All in all, regarding objective 2 it can be said that positioning is influenced by SCR values. Also, residual error graphs and ellipsoidal error analysis graphs are important in understanding the accuracy of the positioning.

6.3. General Discussion

Overall, a comprehensive analysis of the corner reflector's performance at Metsähovi and Loviisa is provided. It also highlights the critical influence of the snow accumulation and temperature variations on their efficiency. Additionally, the accuracy of their positioning has also been examined. This study provided a valuable insight into the behavior of these reflectors under varying environmental conditions.

Objective 1 focused on the impact of snow on SCR values. The correlation between snowfall and SCR values illustrates the profound impact of snow on reflector performance. Loviisa's reflector, while efficient, exhibited fluctuations in SCR values, particularly in response to natural snowmelt.

Objective 2 delved into precise positioning of these reflectors. Metsähovi and Loviisa both showed quite accurate positioning with residual error analysis offering further insights. Notable anomalies in late November for Metsähovi and early December for Loviisa need specific attention for potential improvements.

7. Conclusion

In summary, this study has provided valuable insights into the crucial factors which are influencing the performance of corner reflectors in remote sensing applications. It is evident that snow accumulation significantly impacts the efficiency of these reflectors. As Metsähovi's corner reflector has been studied many times it can be established as a reliable benchmark for validating its suitability for comparative analysis. Comparing Loviisa's reflector with Metsähovi's, similar Signal to clutter (SCR) values were observed, affirming Loviisa's efficiency. However, exceptions arose during extreme snow conditions, when snow accumulation hindered its ability to effectively transmit radio waves. This shows the importance of regular maintenance, especially during heavy snowfall periods.

It has been found that the positioning accuracy is indirectly influenced by snow accumulation, hinges on the strength of the reflected signal, i.e., SCR values. It is important to apply corrections carefully, including tropospheric, ionospheric, and geodynamic corrections, as these directly impact reflector positioning. Additionally, outliers in data may arise, potentially from incorrect pixel selection. To address this, it is recommended to exclude the time containing the outlier and reprocess the data.

Furthermore, an interesting observation regarding reflector positioning has also been highlighted. In cases where exact reference coordinates may not be known, the brightest peak in SAR imagery can be identified by adjusting window size, provided the image has low noise levels. While this approach proved feasible for Metsähovi due to limited brighter pixels, Loviisa's site presented challenges due to an unexpected abundance of brighter pixels as can be seen in figure 11(b). Thus, in such scenarios, an accuracy of 2-3 meters is needed for coordinate determination.

Notably, in Metsähovi, an outlier led to a slight offset in positioning, approximately 2 meters which is higher than expected.

For future studies, the testing scope can be expanded and other seven corner reflectors of Finland can be examined which can then help in providing a more comprehensive understanding of their performance in various geographical and environmental settings. Additionally, managing outliers in the data is crucial for accurate reflector positioning. Careful identification and exclusion of data points associated with outliers, followed by reprocessing is recommended to ensure reliable results.

Furthermore, conducting a comprehensive analysis that goes beyond snow accumulation is essential. Exploring the impact of other environmental variables such as atmospheric conditions on the performance of corner reflectors can also help in understanding their suitability for different geodetic measurements.

8. References

Ao, D., Li, Y., Hu, C., & Tian, W. (2017). Accurate Analysis of Target Characteristic in Bistatic SAR Images: A Dihedral Corner Reflectors Case. *Sensors*, *18*(2), 24. https://doi.org/10.3390/s18010024

Aragones, D., Rodriguez-Galiano, V.F., Caparros-Santiago, J.A. and Navarro-Cerrillo, R.M., 2019. Could land surface phenology be used to discriminate Mediterranean pine species? *International Journal of Applied Earth Observation and Geoinformation*, *78*, pp.281-294.https://www.sciencedirect.com/science/article/pii/S0303243418307335

Balz, T. and Rocca, F., 2020. Reproducibility and replicability in SAR remote sensing. *IEEE Journal of Selected Topics in Applied Earth Observations and Remote Sensing*, *13*, pp.3834-3843.https://ieeexplore.ieee.org/abstract/document/9130105/

Bovenga, F., Refice, A., & Pasquariello, G. (2012). Using corner reflectors and X-band SAR interferometry for slope instability monitoring. *2012 Tyrrhenian Workshop on Advances in Radar and Remote Sensing (TyWRRS)*, 114–120. https://doi.org/10.1109/TyWRRS.2012.6381114

Bovenga, F., Refice, A., Pasquariello, G., Nitti, D. O., & Nutricato, R. (2014). *Corner reflectors and multi-temporal SAR inteferometry for landslide monitoring* (C. Notarnicola, S. Paloscia, & N. Pierdicca, Eds.; p. 92430I). https://doi.org/10.1117/12.2066833

Brock, B.C. and Doerry, A.W., 2009. *Radar cross section of triangular trihedral reflector with extended bottom plate* (No. SAND2009-2993). Sandia National Laboratories (SNL), Albuquerque, NM, and Livermore, CA (United States). https://doi.org/10.2172/984946

Capolongo, D., Refice, A., Bocchiola, D., D'addabbo, A., Vouvalidis, K., Soncini, A., Zingaro, M., Bovenga, F. and Stamatopoulos, L., 2019. Coupling multitemporal remote sensing with geomorphology and hydrological modeling for post flood recovery in the Strymonas dammed river basin (Greece). *Science of the Total Environment*, *651*, pp.1958-1968. https://doi.org/10.1016/j.scitotenv.2018.10.114

Chen, P.H. and Dowman, I.J., 2001. A weighted least squares solution for space intersection of spaceborne stereo SAR data. *IEEE Transactions on Geoscience and Remote Sensing*, *39*(2), pp.233-240. https:// doi.org/10.1109/36.905231.

Chen, L., Tan, S., Pan, Z., Xing, J., Yuan, Z., Xing, X., & Zhang, P. (2020). A New Framework for Automatic Airports Extraction from SAR Images Using Multi-Level Dual Attention Mechanism. *Remote Sensing 2020, Vol. 12, Page 560*, *12*(3), 560. https://doi.org/10.3390/RS12030560

Chen, S. W., Wang, X. S., & Sato, M. (2016). Urban Damage Level Mapping Based on Scattering Mechanism Investigation Using Fully Polarimetric SAR Data for the 3.11 East Japan Earthquake. *IEEE Transactions on Geoscience and Remote Sensing*, *54*(12), 6919–6929. https://doi.org/10.1109/TGRS.2016.2588325

Coletta, A., Angino, G., Battazza, F., Caltagirone, F., Impagnatiello, F., Valentini, G., Capuzi, A., Fagioli, S. and Leonardi, R., 2007, April. COSMO-SkyMed program: Utilization and description of an advanced space EO dual-use asset. In *Proc. Envisat Symp* (pp. 23-27).

Czikhardt, R., van der Marel, H., van Leijen, F. J., & Hanssen, R. F. (2022). Estimating Signal-to-Clutter Ratio of InSAR Corner Reflectors From SAR Time Series. *IEEE Geoscience and Remote Sensing Letters*, *19*, 1–5. https://doi.org/10.1109/LGRS.2021.3070045

Da Silva, A. de Q., Paradella, W. R., Freitas, C. C., & Oliveira, C. G. (2013). Evaluation of Digital Classification of Polarimetric SAR Data for Iron-Mineralized Laterites Mapping in the Amazon Region. *Remote Sensing 2013, Vol. 5, Pages 3101-3122*, *5*(6), 3101–3122. https://doi.org/10.3390/RS5063101

De Alban, J. D. T., Connette, G. M., Oswald, P., & Webb, E. L. (2018). Combined Landsat and L-Band SAR Data Improves Land Cover Classification and Change Detection in Dynamic Tropical Landscapes. *Remote Sensing 2018, Vol. 10, Page 306*, *10*(2), 306. https://doi.org/10.3390/RS10020306

De Luca, G., N. Silva, J.M., Cerasoli, S., Araújo, J., Campos, J., Di Fazio, S. and Modica, G., 2019. Object-based land cover classification of cork oak woodlands using UAV imagery and Orfeo ToolBox. *Remote Sensing*, *11*(10), p.1238. https://doi.org/10.3390/rs11101238

Döring, B., Schwerdt, M. and Bauer, R., 2007. TerraSAR-X calibration ground equipment. *Wave Propagation in Communication, Microwaves Systems and Navigation (WFMN)*. https://doi.org/10.2172/984946

Dyurgerov, M. B., & Meier, M. F. (2000). Twentieth century climate change: Evidence from small glaciers. *Proceedings of the National Academy of Sciences of the United States of America*, *97*(4), 1406–1411. https://doi.org/10.1073/PNAS.97.4.1406

NRSC (2023) *Microwave targets*. Available at: https://www.nrsc.gov.in/EOS_CAL_MicrowaveTargets (accessed: 7 October 2023)

Ferretti, A., Savio, G., Barzaghi, R., Borghi, A., Musazzi, S., Novali, F., Prati, C. and Rocca, F., 2007. Submillimeter accuracy of InSAR time series: Experimental validation. *IEEE Transactions on Geoscience and Remote Sensing*, *45*(5), pp.1142-1153. https://ieeexplore.ieee.org/abstract/document/4156314/

Ferretti, A., Savio, G., Barzaghi, R., Borghi, A., Musazzi, S., Novali, F., Prati, C. and Rocca, F., 2007. Submillimeter accuracy of InSAR time series: Experimental validation. *IEEE Transactions on Geoscience and Remote Sensing*, *45*(5), pp.1142-1153.

Fu, W., Guo, H., Tian, Q., & Guo, X. (2010). Landslide monitoring by corner reflectors differential interferometry SAR. *International Journal of Remote Sensing*, *31*(24), 6387–6400. https://doi.org/10.1080/01431160903413713

Garthwaite, M. C., Thankappan, M., Williams, M. L., Nancarrow, S., Hislop, A., & Dawson, J. (2013). Corner reflectors for the Australian Geophysical Observing System and support for calibration of satellite-borne synthetic aperture radars. *International Geoscience and Remote Sensing Symposium (IGARSS)*, 266–269. https://doi.org/10.1109/IGARSS.2013.6721143

Garthwaite, M.C., Nancarrow, S., Hislop, A., Thankappan, M., Dawson, J.H. and Lawrie, S., 2015a. Design of radar corner reflectors for the Australian Geophysical Observing System. *Geoscience Australia*, *3*, p.490. https://doi.org/10.11636/Record.2015.003

Garthwaite, M.C., Lawrie, S., Dawson, J. and Thankappan, M., 2015b. Corner reflectors as the tie between InSAR and GNSS measurements: Case study of resource extraction in Australia. *Eur. Sp. Agency. Spec. Publ., ESA SP SP-731*. https://doi.org/10.5270/Fringe2015.pp60

Garthwaite, M.C., Nancarrow, S., Hislop, A., Thankappan, M., Dawson, J.H. and Lawrie, S., 2015. Design of radar corner reflectors for the Australian Geophysical Observing System. *Geoscience Australia*, *3*, p.490. https://doi.org/10.11636/Record.2015.003

Gisinger, C. (2020). *SAR Imaging Geodesy - Towards Absolute Coordinates with Centimeter Accuracy*. http://mediatum.ub.tum.de/?id=1473711

Gisinger, C., Schubert, A., Breit, H., Garthwaite, M., Balss, U., Willberg, M., Small, D., Eineder, M., & Miranda, N. (2021). In-Depth Verification of Sentinel-1 and TerraSAR-X Geolocation Accuracy Using the Australian Corner Reflector Array. *IEEE Transactions on Geoscience and Remote Sensing*, *59*(2), 1154–1181. https://doi.org/10.1109/TGRS.2019.2961248

Gisinger, C., Willberg, M., Balss, U., Klügel, T., Mähler, S., Pail, R., & Eineder, M. (2017). Differential geodetic stereo SAR with TerraSAR-X by exploiting small multi-directional radar reflectors. *Journal of Geodesy*, *91*(1), 53–67. https://doi.org/10.1007/S00190-016-0937-2/FIGURES/11

Goffi, A., Stroppiana, D., Brivio, P. A., Bordogna, G., & Boschetti, M. (2020). Towards an automated approach to map flooded areas from Sentinel-2 MSI data and soft integration of water spectral features. *International Journal of Applied Earth Observation and Geoinformation*, *84*. https://doi.org/10.1016/J.JAG.2019.101951

Grabska, E., Hawryło, P. and Socha, J., 2020. Continuous detection of small-scale changes in scots pine dominated stands using dense sentinel-2 time series. *Remote Sensing*, *12*(8), p.1298. https://doi.org/10.3390/rs12081298

Grabska, E., Hostert, P., Pflugmacher, D., & Ostapowicz, K. (2019). Forest Stand Species Mapping Using the Sentinel-2 Time Series. *Remote Sensing*, *11*(10), 1197. https://doi.org/10.3390/rs11101197

Gruber, T., Ågren, J., Angermann, D., Ellmann, A., Engfeldt, A., Gisinger, C., Jaworski, L., Kur, T., Marila, S., Nastula, J., Nilfouroushan, F., Nordman, M., Poutanen, M., Saari, T., Schlaak, M., Świątek, A., Varbla, S., & Zdunek, R. (2022). Geodetic SAR for Height System Unification and Sea Level Research—Results in the Baltic Sea Test Network. *Remote Sensing 2022, Vol. 14, Page 3250*, *14*(14), 3250. https://doi.org/10.3390/RS14143250

He, B., Xing, M., & Bai, X. (2014). A Synergistic Methodology for Soil Moisture Estimation in an Alpine Prairie Using Radar and Optical Satellite Data. *Remote Sensing 2014, Vol. 6, Pages 10966-10985*, *6*(11), 10966–10985. https://doi.org/10.3390/RS61110966

Huang, L., Liu, B., Li, X., Zhang, Z., & Yu, W. (2017). Technical Evaluation of Sentinel-1 IW Mode Cross-Pol Radar Backscattering from the Ocean Surface in Moderate Wind Condition. *Remote Sensing 2017, Vol. 9, Page 854*, *9*(8), 854. https://doi.org/10.3390/RS9080854

Huang, M., & Jin, S. (2020). Rapid Flood Mapping and Evaluation with a Supervised Classifier and Change Detection in Shouguang Using Sentinel-1 SAR and Sentinel-2 Optical Data. *Remote Sensing*, *12*(13), 2073. https://doi.org/10.3390/rs12132073

Javali, A., Gupta, J., & Sahoo, A. (2021). A review on Synthetic Aperture Radar for Earth Remote Sensing: Challenges and Opportunities. *2021 Second International Conference on Electronics and Sustainable Communication Systems (ICESC)*, 596–601. https://doi.org/10.1109/ICESC51422.2021.9532910

Kausarian, H., Sri Sumantyo, J. T., Kuze, H., Aminuddin, J., & Waqar, M. M. (2017). Analysis of Polarimetric Decomposition, Backscattering Coefficient, and Sample Properties for Identification and Layer Thickness Estimation of Silica Sand Distribution Using L-Band Synthetic Aperture Radar. *Http://Dx.Doi.Org/10.1080/07038992.2017.1286935*, *43*(2), 95–108. https://doi.org/10.1080/07038992.2017.1286935

Koppe, W., Wenzel, R., Hennig, S., Janoth, J., Hummel, P., & Raggam, H. (2012). Quality assessment of TerraSAR-X derived ground control points. *International Geoscience and Remote Sensing Symposium (IGARSS)*, 3580–3583. https://doi.org/10.1109/IGARSS.2012.6350643

Lapini, A., Pettinato, S., Santi, E., Paloscia, S., Fontanelli, G. and Garzelli, A., 2020. Comparison of machine learning methods applied to SAR images for forest classification in mediterranean areas. *Remote Sensing*, *12*(3), p.369. https://doi.org/10.3390/rs12030369

Li, Y., Martinis, S., Plank, S., & Ludwig, R. (2018). An automatic change detection approach for rapid flood mapping in Sentinel-1 SAR data. *International Journal of Applied Earth Observation and Geoinformation*, *73*, 123–135. https://doi.org/10.1016/J.JAG.2018.05.023

Liu, G., Yang, X., Li, X., Zhang, B., Pichel, W., Li, Z., & Zhou, X. (2013). A Systematic Comparison of the Effect of Polarization Ratio Models on Sea Surface Wind Retrieval From C-Band Synthetic Aperture Radar. *IEEE Journal of Selected Topics in Applied Earth Observations and Remote Sensing*, *6*(3), 1100–1108. https://doi.org/10.1109/JSTARS.2013.2242848

Marinkovic, P., Ketelaar, G., van Leijen, F. and Hanssen, R., 2007, November. InSAR quality control: Analysis of five years of corner reflector time series. In *Proceedings of the Fringe 2007 Workshop (ESA SP-649), Frascati, Italy* (pp. 26-30).

Martinis, S., Rieke, C., J-P Schumann, G., Balzter, H., & Thenkabail, P. S. (2009). Backscatter analysis using multi-temporal and multi-frequency SAR data in the context of flood mapping at River Saale, Germany. *Mdpi.Com*, *7*(6), 7732–7752. https://doi.org/10.3390/rs70607732

Marzialetti, F., Giulio, S., Malavasi, M., Sperandii, M.G., Acosta, A.T.R. and Carranza, M.L., 2019. Capturing coastal dune natural vegetation types using a phenology-based mapping approach: The potential of Sentinel-2. *Remote Sensing*, *11*(12), p.1506. https://doi.org/10.3390/rs11121506

Nicolau, A.P., Flores-Anderson, A., Griffin, R., Herndon, K. and Meyer, F.J., 2021. Assessing SAR C-band data to effectively distinguish modified land uses in a heavily disturbed Amazon forest. *International Journal of Applied Earth Observation and Geoinformation*, *94*, p.102214. https://www.sciencedirect.com/science/article/pii/S0303243420302579

Nie, J., Xu, Q., Pan, J., & Guo, M. (2022). Hyperspectral Image Classification Based on Multiscale Spectral-Spatial Deformable Network. *IEEE Geoscience and Remote Sensing Letters*, *19*. https://doi.org/10.1109/LGRS.2020.3024006

Nitti, D. O., Morea, A., Nutricato, R., Chiaradia, M. T., La Mantia, C., Agrimano, L., & Samarelli, S. (2016). *Automatic GCP extraction with high resolution COSMO-SkyMed products* (C. Notarnicola, S. Paloscia, N. Pierdicca, & E. Mitchard, Eds.; p. 1000302). https://doi.org/10.1117/12.2241281

Onisi Kirubanandam, N., & Raju, G. (2019). Preliminary studies on corner reflectors responses as seen in Sentinel-1A images over Kanakapura region. *Journal of the Indian Society of Remote Sensing*, *47*(1), 25–32. https://doi.org/10.1007/S12524-018-0860-5/FIGURES/5

Park, S.-E., Yamaguchi, Y., & Kim, D.-J. (2013). *Polarimetric SAR remote sensing of the 2011 Tohoku earthquake using ALOS/PALSAR*. https://doi.org/10.1016/j.rse.2013.01.018

Parker, A.L., Featherstone, W.E., Penna, N.T., Filmer, M.S. and Garthwaite, M.C., 2017. Practical considerations before installing ground-based geodetic infrastructure for integrated InSAR and cGNSS monitoring of vertical land motion. *Sensors*, *17*(8), p.1753. https://doi.org/10.3390/s17081753

Pawłuszek-Filipiak, K., Wielgocka, N., Tondaś, D. and Borkowski, A., 2023. Monitoring nonlinear and fast deformation caused by underground mining exploitation using multi-temporal Sentinel-1 radar interferometry and corner reflectors: application, validation and processing obstacles. *International Journal of Digital Earth*, *16*(1), pp.251-271. https://doi.org/10.1080/17538947.2023.2166607

Marinkovic, P., Ketelaar, G., van Leijen, F. and Hanssen, R., 2007, November. InSAR quality control: Analysis of five years of corner reflector time series. In *Proceedings of the Fringe 2007 Workshop (ESA SP-649), Frascati, Italy* (pp. 26-30).

Flores-Anderson, A.I., Herndon, K.E., Thapa, R.B. and Cherrington, E., 2019. *The SAR handbook: Comprehensive methodologies for forest monitoring and biomass estimation* (No. MSFC-E-DAA-TN67454).

Pedroso, E. C., Rivard, B., Crósta, A. P., Filho, C. R. D. S., & Miranda, F. P. (2014). Reconnaissance Geologie Mapping in the Tapajós Mineral Province, Brazilian Amazon, Using Spaceborne SAR Imagery and Airborne Geophysics. https://doi.Org/10.1080/07038992.2001.10854909, 27(6), 669–678.

Praks, J. (2012). *Radar polarimetry and interferometry for remote sensing of boreal forest*. http://urn.fi/URN:ISBN:978-952-60-4873-4

Praticò, S., Solano, F., Di Fazio, S. and Modica, G., 2021. Machine learning classification of mediterranean forest habitats in google earth engine based on seasonal sentinel-2 time-series and input image composition optimisation. *Remote Sensing*, *13*(4), p.586. https://doi.org/10.3390/rs13040586

Chen, P.H. and Dowman, I.J., 2001. A weighted least squares solution for space intersection of spaceborne stereo SAR data. *IEEE Transactions on Geoscience and Remote Sensing*, *39*(2), pp.233-240. https://doi.org/10.1109/36.905231

Qin, Y., Perissin, D., & Lei, L. (2013). The Design and Experiments on Corner Reflectors for Urban Ground Deformation Monitoring in Hong Kong. *International Journal of Antennas and Propagation*, *2013*, 1–8. https://doi.org/10.1155/2013/191685

Raggam, H., Perko, R., Gutjahr, K., Bayerische, N. K., & Aör, S. (2010). *Accuracy Assessment of 3D Point Retrieval from TerraSAR-X Data Sets Sentinel 2 Global Mosaics-Validation View project COPERNICUS Land Monitoring Service-Improvement View project*. https://www.researchgate.net/publication/224233726

Romeiser, R. (2013). The Future of SAR-Based Oceanography: High-Resolution Current Measurements by Along-Track Interferometry. *Oceanography*, *26*(2). https://doi.org/10.5670/OCEANOG.2013.37

Rostami, M., Kolouri, S., Eaton, E., & Kim, K. (2019). Deep Transfer Learning for Few-Shot SAR Image Classification. *Remote Sensing 2019, Vol. 11, Page 1374*, *11*(11), 1374. https://doi.org/10.3390/RS11111374

Schiller, S., Gruber, T. and Schlaak, M., 2023. First Evaluation of Swedish and Finnish Corner Reflectors. In *Workshop on the Geodetic Applications of Synthetic Aperture Radar*. https://mediatum.ub.tum.de/doc/1704036/document.pdf

Shangguan, M., Wang, W., & Jin, S. (2019). Variability of temperature and ozone in the upper troposphere and lower stratosphere from multi-satellite observations and reanalysis data. *Atmospheric Chemistry and Physics*, *19*(10), 6659–6679. https://doi.org/10.5194/ACP-19-6659-2019

Shen, H., He, Y., & Perrie, W. (2009). Speed ambiguity in hurricane wind retrieval from SAR imagery. *Http://Dx.Doi.Org/10.1080/01431160802555879*, *30*(11), 2827–2836. https://doi.org/10.1080/01431160802555879

Shen, H., Perrie, W., & Wu, Y. (2019). Wind drag in oil spilled ocean surface and its impact on wind-driven circulation. *Anthropocene Coasts*, *2*(1), 244–260. https://doi.org/10.1139/ANC-2018-0019/ASSET/IMAGES/LARGE/ANC-2018-0019F7.JPEG

Shen, X., Anagnostou, E. N., Allen, G. H., Robert Brakenridge, G., & Kettner, A. J. (2019). Near-real-time non-obstructed flood inundation mapping using synthetic aperture radar. *Remote Sensing of Environment*, *221*, 302–315. https://doi.org/10.1016/J.RSE.2018.11.008

Shu, G., Wang, N., Wang, W., Deng, Y., Zhang, Y., Zhang, H., Li, N. and Wang, R., 2021. A novel vortex synthetic aperture radar imaging system: decreasing the pulse repetition frequency without increasing the antenna aperture. *IEEE Transactions on Geoscience and Remote Sensing*, *60*, pp.1-14. https://ieeexplore.ieee.org/abstract/document/9366953/

Singha, S., Velotto, D., & Lehner, S. (2014). Near real time monitoring of platform sourced pollution using TerraSAR-X over the North Sea. *Marine Pollution Bulletin*, *86*(1–2), 379–390. https://doi.org/10.1016/J.MARPOLBUL.2014.06.041

Solano, F., Colonna, N., Marani, M. and Pollino, M., 2019. Geospatial analysis to assess natural park biomass resources for energy uses in the context of the rome metropolitan area. In *New Metropolitan Perspectives: Local Knowledge and Innovation Dynamics Towards Territory Attractiveness Through the Implementation of Horizon/E2020/Agenda2030–Volume 1* (pp. 173-181). Springer International Publishing. https://doi.org/10.1007/978-3-319-92099-3_21

Spracklen, B. and Spracklen, D.V., 2021. Synergistic Use of Sentinel-1 and Sentinel-2 to map natural forest and acacia plantation and stand ages in North-Central Vietnam. *Remote Sensing*, *13*(2), p.185. https://doi.org/10.3390/rs13020185

Stastny, J., Cheung, S., Wiafe, G., Agyekum, K. and Greidanus, H., 2014. Application of RADAR corner reflectors for the detection of small vessels in synthetic aperture radar. *IEEE Journal of Selected Topics in Applied Earth Observations and Remote Sensing*, *8*(3), pp.1099-1107.

Synthetic Aperture Radar (EUSAR), 2010 8th European Conference on: date, 7-10 June 2010.

Topouzelis, K., & Psyllos, A. (2012). Oil spill feature selection and classification using decision tree forest on SAR image data. *ISPRS Journal of Photogrammetry and Remote Sensing*, *68*(1), 135–143. https://doi.org/10.1016/J.ISPRSJPRS.2012.01.005

Tsokas, A., Rysz, M., Pardalos, P. M., & Dipple, K. (2022). SAR data applications in earth observation: An overview. *Expert Systems With Applications*, *205*, 117342. https://doi.org/10.1016/j.eswa.2022.117342

Ulaby, F. T., Aslam, A., & Dobson, M. C. (1982). Effects of Vegetation Cover on the Radar Sensitivity to Soil Moisture. *IEEE Transactions on Geoscience and Remote Sensing*, *GE-20*(4), 476–481. https://doi.org/10.1109/TGRS.1982.350413 van Genderen, J. (2016). Fundamentals of satellite remote sensing: an environmental approach. *International Journal of Digital Earth*, *9*(12), 1275–1276. https://doi.org/10.1080/17538947.2016.1209938

Wang, J., Lu, C., & Jiang, W. (2018). Simultaneous Ship Detection and Orientation Estimation in SAR Images Based on Attention Module and Angle Regression. *Sensors 2018, Vol. 18, Page 2851*, *18*(9), 2851. https://doi.org/10.3390/S18092851

Wang, Z., Li, Y., Yu, F., Yu, W., Jiang, Z., & Ding, Y. (2016). Object detection capability evaluation for SAR image. *International Geoscience and Remote Sensing Symposium (IGARSS)*, *2016-November*, 1548–1551. https://doi.org/10.1109/IGARSS.2016.7729395

Watanabe, M., Thapa, R. B., Ohsumi, T., Fujiwara, H., Yonezawa, C., Tomii, N., & Suzuki, S. (2016). Detection of damaged urban areas using interferometric SAR coherence change with PALSAR-2 4. Seismology. *Earth, Planets and Space*, *68*(1), 1–12. https://doi.org/10.1186/S40623-016-0513-2/FIGURES/8

Werninghaus, R., & Buckreuss, S. (2010). The TerraSAR-X Mission and System Design. *IEEE Transactions on Geoscience and Remote Sensing*, *48*(2), 606–614. https://doi.org/10.1109/TGRS.2009.2031062

What is a Corner Reflector? - everything RF. (2023). Retrieved July 5, 2023, from https://www.everythingrf.com/community/what-is-a-corner-reflector

Xiong, C., Shi, J., Pan, J., Xu, H., Che, T., Zhao, T., Ren, Y., Geng, D., Chen, T., Jiang, K. and Feng, P., 2021. Time Series X-and Ku-Band Ground-Based Synthetic Aperture Radar Observation of Snow-Covered Soil and Its Electromagnetic Modeling. *IEEE Transactions on Geoscience and Remote Sensing*, *60*, pp.1-13. https://ieeexplore.ieee.org/abstract/document/9410268/

Yahia, M., Ali, T., Mortula, M.M., Abdelfattah, R. and El Mahdy, S., 2020. Polarimetric SAR speckle reduction by hybrid iterative filtering. *IEEE Access*, *8*, pp.89603-89616. https://ieeexplore.ieee.org/abstract/document/9091157/

Ye, X., Kaufmann, H., & Guo, X. F. (2004). Landslide Monitoring in the Three Gorges Area Using D-INSAR and Corner Reflectors. *Photogrammetric Engineering & Remote Sensing*, *70*(10), 1167–1172. https://doi.org/10.14358/PERS.70.10.1167

Ye, X., Lin, M., Yuan, X., Ding, J., Xie, X., Zhang, Y., & Xu, Y. (2016). Satellite SAR observation of the sea surface wind field caused by rain cells. *Acta Oceanologica Sinica*, *35*(9), 80–85. https://doi.org/10.1007/S13131-016-0936-4/METRICS

Xia, Y., Kaufmann, H. and Guo, X., 2002, June. Differential SAR interferometry using corner reflectors. In *IEEE International Geoscience and Remote Sensing Symposium* (Vol. 2, pp. 1243-1246). IEEE.

Zhang, B., Perrie, W., & He, Y. (2011). Wind speed retrieval from RADARSAT-2 quad-polarization images using a new polarization ratio model. *Journal of Geophysical Research*, *116*(C8), C08008. https://doi.org/10.1029/2010JC006522

Zhang, H., Zhang, Y., & Lin, H. (2012). A comparison study of impervious surfaces estimation using optical and SAR remote sensing images. *International Journal of Applied Earth Observation and Geoinformation*, *18*, 148–156. https://doi.org/10.1016/j.jag.2011.12.015

Zheng, Q., Zhao, Q., Yuan, Y., Liu, X., Hu, J., Liu, X., Yin, L., & Ye, X. (2012). Shear-flow induced secondary circulation in parallel underwater topographic corrugation and its application to satellite image interpretation. *Journal of Ocean University of China*, *11*(4), 427–435. https://doi.org/10.1007/S11802-012-2093-5/METRICS

Zhou, Y., Wang, P., Chen, Z., Zhao, Q., Wang, W., Zhang, L., Yu, W., Deng, Y. and Wang, R., 2020. Very high resolution SAR imaging with DGPS-supported airborne X-band data. *IEEE Journal of Selected Topics in Applied Earth Observations and Remote Sensing*, *13*, pp.3605-3617. https://ieeexplore.ieee.org/abstract/document/9122449/

Zhu, Q., Jiang, W., Zhu, Y., & Li, L. (2020). Geometric Accuracy Improvement Method for High-Resolution Optical Satellite Remote Sensing Imagery Combining Multi-Temporal SAR Imagery and GLAS Data. *Remote Sensing 2020, Vol. 12, Page 568*, *12*(3), 568. https://doi.org/10.3390/RS12030568